Numerical Investigation of Hydrodynamic Loads for Subsea Structures

A.M Deshpande
5631971

MSc. Offshore and Dredging Engineering

Delft University of Technology

Masters Thesis

Numerical Investigation of Hydrodynamic Loads for Subsea Structures

by

A.M. Deshpande

to obtain the degree of Master of Science

at the Delft University of Technology,

to be defended publicly on Thursday February 27, 2025 at 14:30 PM.

Student number:	5631971	
Project duration:	May 1, 2023 – May 1, 2024	
Thesis committee:	Dr. Ir. K. Anupam	TU Delft, chair, supervisor
	Dr. Ir. A. Cabboi,	TU Delft, external
	Ir. A. Wagasing Arachchige	TU Delft
	Ir. T. Dronkers	Allseas Engineering B.V.

Allseas

TU Delft

Acknowledgments

The completion of this thesis would not have been possible without the invaluable support and guidance received throughout this academic journey.

First and foremost, sincere gratitude is extended to Dr. Kumar Anupam, the chair of the thesis committee, supervisor, and mentor. His expertise in Computational Fluid Dynamics (CFD) and Structural Engineering has been instrumental in shaping this research. His unwavering support, insightful feedback, and patient guidance have provided clarity and direction throughout this work. Beyond his role as a supervisor, he has also served as a mentor, imparting invaluable lessons in research approach, critical thinking, and professional as well as personal development.

Appreciation is also extended to the company supervisor, Unit Head Engineering, Thomas Dronkers, from Allseas, whose introduction to this thesis opportunity and support within the Pipeline Engineering Group in Delft have been greatly valued. His continuous encouragement, constructive feedback, and belief in the potential of this research have played a significant role in refining its scope and depth. His guidance from the project initiation to the final review has been invaluable. Special thanks are also extended to Robby van Vliet, Installation Engineer and Mehdi Ghodossi, Principal Engineer, for their technical insights, guidance, patience, and willingness to provide support throughout the research lifecycle.

Heartfelt appreciation is extended to my friends and colleagues at Allseas and TU Delft for their collaboration, encouragement, motivation and shared knowledge, which contributed significantly to both personal and academic growth. The supportive and stimulating environment fostered within the Pipeline Engineering team at Allseas in Delft made this research an enriching experience. Likewise, the debates and discussions with peers at TU Delft provided essential motivation and birds eye perspective throughout this masters academic journey.

Finally, profound gratitude is expressed to my family and close friends for their unwavering support, patience, and belief in this endeavor. Their encouragement during challenges and perseverance has been a constant source of motivation for me personally.

To all who contributed to this work, either directly or indirectly, sincere thanks are extended for being part of this special meaningful journey.

A.M. Deshpande
Delft, February 2025

Executive Summary

This research investigates the integration of Computational Fluid Dynamics (CFD) with industry-standard guidelines, such as DNV, to improve hydrodynamic load predictions for a J-lay Pipeline End Terminal (PLET) installation under high sea states. The study evaluates whether CFD-derived drag and added mass coefficients can enhance the accuracy of dynamic installation simulations and improve workability.

The methodology follows a staged validation process, beginning with 2D steady-flow simulations of thin flat plates to establish confidence in the CFD approach. This is followed by full-scale simulations of simplified subsea structures, including mud mats, in both 2D and 3D. The transition to 3D modeling is necessary to capture spanwise vortex shedding and realistic flow separations. Added mass effects are analyzed using oscillatory flow simulations, with coefficients extracted through a least-squares fitting approach to Morison's equation.

The results indicate that CFD-derived coefficients generally align with DNV values but show variations depending on orientation and aspect ratio. Incorporating these coefficients into dynamic installation simulations leads to a 10% reduction in bending strains compared to estimates using DNV values. While this demonstrates CFD's potential to refine hydrodynamic predictions, the improvements remain moderate, suggesting that CFD serves as a complementary tool rather than a replacement for empirical guidelines. The study highlights that CFD provides refined hydrodynamic insights, but its applicability is limited by computational resources and modeling assumptions.

Several limitations affect the study, including simplified environmental conditions, standard turbulence modeling, and restricted added mass simulations due to computational constraints. Future research should focus on incorporating free-surface effects, refining turbulence models, increasing mesh resolution, and validating results through experimental or in-situ field data.

Overall, the findings demonstrate that CFD can enhance hydrodynamic load predictions, though its effectiveness depends on site specificenvironmental conditions. Further advancements in computational modeling and validation will be essential to improving offshore installation planning and design.

Contents

List of Figures

List of Tables

1

Introduction

1.1. Background

The offshore oil and gas industry remains a fundamental component of the global energy supply, significantly contributing to hydrocarbon production [1]. Since the first offshore well was drilled in the Gulf of Mexico in 1947 [2], continuous advancements have been made to meet rising energy demands. This progress has necessitated exploration and production activities in increasingly challenging and remote environments, including deepwater regions [3].

To enable operations in such extreme conditions, advancements in subsea engineering have become essential [4]. Subsea engineering is a specialized field focused on the design, installation, and operation of equipment deployed beneath the ocean surface [5]. Modern subsea production systems, as depicted in Figure 1.1, are composed of large, rigid structural assemblies designed to extract and transport hydrocarbons and natural gas from reservoirs beneath the seabed. These systems incorporate rigid pipelines, manifolds, jumpers, risers, subsea trees, mudmats, roller guides, pipeline end termination units (PLETs), and pipeline end manifolds (PLEMs) [6]. Among these, PLETs serve as weight-bearing structures that connect subsea pipeline ends, while PLEMs act as hubs that facilitate oil and gas flow by interconnecting multiple pipelines [7].

The reliability of these subsea structures is contingent on their ability to withstand hydrodynamic loads induced by harsh metocean conditions, which include wind-generated waves, storm surges, currents, tides, and temperature variations [8]. These environmental factors influence the design, installation, and operation of subsea systems, impacting structural integrity, fatigue life, and hydrodynamic loading throughout installation and operational phases.

The installation of subsea structures in deep-water environments presents considerable challenges due to the interplay of environmental forces and technical design constraints [6]. To address these challenges, specialized pipeline installation methods, including S-lay, J-lay, and Reel-lay, have been developed. The S-lay method, suitable for shallow to moderate depths, involves laying the pipeline in an elongated 'S' shape from the vessel to the seabed. The J-lay method, optimized for deep-water applications, deploys the pipeline in a near-vertical orientation resembling the letter 'J.' In contrast, the Reel-lay method entails

spooling the pipeline onto a large reel on the vessel and subsequently unspooling it onto the seabed, allowing for rapid installation under specific pipeline configurations [9, 5]. Despite these advancements, the design and installation of subsea structures continue to be constrained by extreme environmental conditions, particularly high sea states.

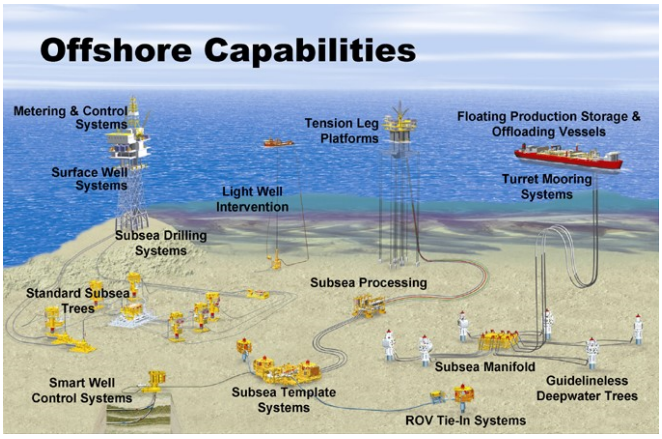

Figure 1.1: A typical subsea production system illustrating key components [1].

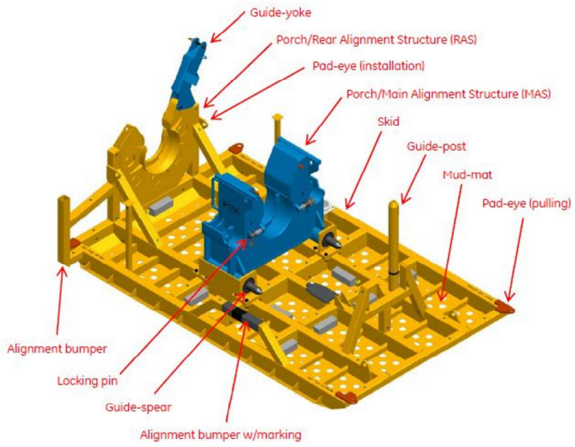

Figure 1.2: A typical open PLET structure with detailed components [7].

1.2. Engineering Challenges

During installation, subsea structures, specifically large PLETs, are subjected to various hydrodynamic forces as they pass through the splash zone—the region near the ocean's surface where waves and currents are most active [10], extending up to the touchdown point near the seabed. The dynamic interaction between ocean waves, currents, and the structure can lead to induced translational and rotational motions and bending stresses due to wave kinematics. Therefore, accurate estimation of hydrodynamic loads such as drag and added mass is crucial for safe and efficient installations and feasibility studies involving the design, installation, and marine operations [11].

Classification societies, such as Det Norske Veritas (DNV), provide industry standards and guidelines for predicting these loads for marine and subsea operations [12]. These standards often rely on simplified analytical and semi-empirical methods based on basic geometrical shapes, such as cylinders,

squares, cubes, and flat plates. Traditional industry-standard methods like Morison's equation are commonly used to estimate hydrodynamic loads on slender structures by combining inertia and drag force components [13]. While practical for preliminary assessments, these methods may only partially capture the complex fluid-structure interactions and nonlinearities of modern subsea structures [14]. Such structures often have intricate geometries and are subjected to combined wave and current effects from all directions [15]. Inaccurate predictions may result in underestimated loading conditions, leading to excessive bending and buckling stresses, potential structural failures, and installation inefficiencies.

This is particularly critical during J-lay PLET installations, where the pipeline undergoes a complex deformation known as the sagbend—the region near the seabed where the pipeline transitions from a vertical to a horizontal orientation [6]. Excessive structural motions and bending strains in the sagbend region can compromise the workability of the installation procedure, especially under higher sea states [9]. In some cases, snap loads may develop due to sudden increases in heave displacement of the structure caused by uneven buoyancy and vessel roll motions. These dynamic impulse loads can lead to slackness in the pipeline catenary and exceed tolerance limits for buckling unity checks [14, 9].

All the above-discussed challenges highlight the limitations of traditional hydrodynamic modeling methods, motivating the development of more advanced frameworks to address the complex fluid-structure interactions present during J-lay PLET installations. Integrating advanced numerical models into the hydrodynamic load prediction process offers the potential to model these interactions with greater accuracy [15]. These models allow for detailed analysis of fluid flow around complex geometries, capturing effects that DNV may overlook [16].

1.3. Research Aim and Objectives

The primary aim of this research is to investigate and improve the hydrodynamic load modeling methodology for J-lay PLET installations by developing and validating a numerical framework that enhances the accuracy of hydrodynamic load predictions for complex subsea structures. To achieve this aim, several key objectives are pursued:

Firstly, a numerical framework integrating advanced computational techniques is developed to calculate hydrodynamic loads, specifically drag and added mass coefficients. Computational Fluid Dynamics (CFD) simulations of two-dimensional scaled thin flat plates under steady flow conditions, replicating constant currents, are utilized to establish the framework's accuracy and reliability. The CFD results are validated against experimental data of a similar thin flat plate to ensure model credibility.

Subsequently, the validated model is extended to three-dimensional full-scale subsea PLET support structures, including mudmats, folded mudmats, and roller guides. Hydrodynamic coefficients for various configurations and aspect ratios relevant to J-lay PLET installations are computed and compared with those derived analytically from DNV standards. This comparison aims to assess discrepancies and identify potential improvements in existing load predictions.

Finally, the improved hydrodynamic coefficients are integrated into time-domain dynamic installation simulations to evaluate their effects on predicted bending strains and structural responses near the sagbend region. This assessment determines the impact and implications of the enhanced hydrodynamic load modeling methodology on the workability of J-lay PLET installations, ultimately contributing to more efficient and reliable offshore and subsea operations.

1.4. Research Scope

This research is confined and limited to improving hydrodynamic load predictions for J-lay PLET installations through the development and validation of a numerical framework. The focus is placed on calculating hydrodynamic coefficients, specifically drag and added mass, for subsea support structures attached to pipelines during J-lay installation. Computational Fluid Dynamics (CFD) is employed as the primary tool within the numerical framework. Realistic metocean conditions relevant to deepwater installations are considered, with steady flow and oscillatory conditions modeled using wave kinematics derived from significant wave heights and peak periods. The reserach also encompasses full-scale symmetric and asymmetric support structures, such as mudmats (flat seabed support structures for stability) and roller guides (pipeline guiding devices during installation) of various aspect ratios, commonly utilized in J-lay PLET installations.

Certain limitations are inherent in the reserach due to simplifications and exclusions. The numerical framework does not account for free surface effects, seabed interactions, or nonlinear free surface wave modeling. The oscillatory nature of wave-induced flows is not modeled for full-scale simulations; instead, steady flow approximations in form of current are utilized. The research does not involve the design optimization of new subsea structures or the development of novel installation techniques. Material properties, geotechnical aspects, and real-time vessel motion dynamics are also excluded from the numerical model development.

1.5. Research Significance

This research contributes to the offshore industry by introducing a numerical framework that aims to improve and enhance the accuracy of hydrodynamic load predictions for complexand simple shaped subsea support structures during J-lay PLET installations. Improved load and coefficient prediction accuracy is expected to mitigate induced structural motions and bending stresses, resulting in efficient operations and increased workability under higher sea states. In addition to optimizing installation procedures, this improvement supports sustainable marine operations by reducing vessel time at sea, thereby decreasing fuel consumption and lowering greenhouse gas emissions. Next, the integration of advanced computational techniques facilitates more efficient resource utilization by minimizing the need for excessively conservative designs and extensive experimental testing, which can contribute to material waste and elevated costs. By establishing a foundation for future studies, this research aims to supports the industry's transition toward sustainable installation engineering practices and kickstart advancements in high- and mid-fidelity numerical simulation methods for offshore and subsea engineering applications [17].

2

Subsea Hydrodynamics: Principles, Methods, and Computational Approaches

This chapter provides an in-depth overview of subsea structures, their installation methods, and the hydrodynamic forces they encounter. Alongside, existing and advanced computational modeling techniques used to predict these forces are explored. The chapter is structured as follows:

- Overview of Subsea Structures
- Installation Techniques
- Fundamental Principles in Hydrodynamics
- Flow Conditions and Their Impact on Hydrodynamic Forces
- Challenges in Modeling Hydrodynamic Loads
- Current Computational Modeling Techniques
- Summary

2.1. Overview of Subsea Structures

Designed to operate under extreme underwater conditions for a lifespan of 25 to 30 years, subsea structures are critical to offshore field development.[18] The installation of these structures requires specialized techniques to ensure structural integrity and operational efficiency [6]. Commonly employed methods include the S-lay and J-lay techniques, each presenting distinct advantages and challenges. The key components of subsea systems are summarized below:

- **Pipelines:** Subsea pipelines transport oil, gas, and occasionally water from subsea wells to surface processing facilities or storage units. These pipelines are engineered to withstand high pressures, corrosive environments, and dynamic marine conditions. Accurate prediction of

hydrodynamic forces, such as drag and inertia, is essential to ensuring their structural and foundational stability [19].

- **Manifolds:** Manifolds serve as junction points where production from multiple wells is collected and routed. These systems regulate the flow of hydrocarbons, optimizing production efficiency. Their design must account for hydrodynamic loads, particularly in deepwater environments, to prevent structural failures [20].
- **Roller Guides:** Roller guides are auxiliary structures used during the installation of subsea pipelines and umbilicals to minimize friction and ensure precise placement. These guides must withstand significant tension and bending forces, which are amplified by hydrodynamic loads from waves and currents [19].

Figure 2.1: Roller guides for pipeline installation [9].

- **Mudmats:** Mudmats provide stable foundations for subsea equipment, such as manifolds, Pipeline End Terminations (PLETs), and subsea trees. Their design ensures even weight distribution to prevent sinking or tilting in soft seabed conditions, while maintaining stability under varying hydrodynamic loads, particularly those related to scour effects induced by currents [20].

Figure 2.2: Mudmat used for subsea equipment support [21].

- **Folded Mudmats:** Folded mudmats are designed to facilitate transport and deployment. These structures can be folded during transit and expanded on-site, ensuring stability under hydrodynamic forces encountered at greater depths [22].

2.2. Installation Methods

The installation of subsea structures, particularly pipelines, requires sophisticated techniques tailored to specific operational conditions, including water depth, seabed characteristics, and structural requirements. The primary methods employed for pipeline installation, as discussed in chapter 1, include S-lay, J-lay, and reel-lay techniques (see Figure 2.3).

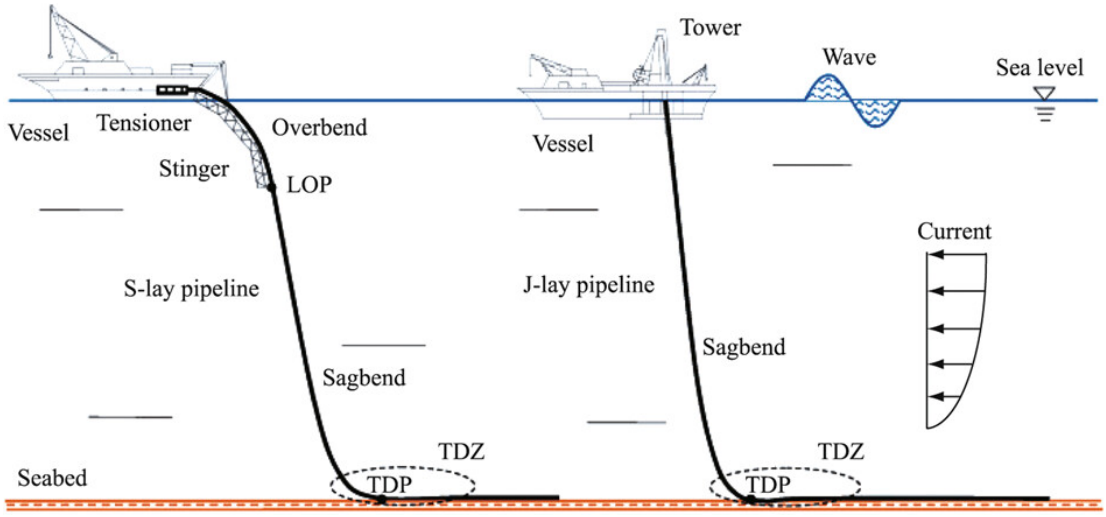

Figure 2.3: Schematic representation of S-lay and J-lay installation methods [9].

S-lay Method

The S-lay method is widely utilized for pipeline installation in shallow to moderately deep waters. In this approach, the pipeline is deployed in an "S" shape from the vessel to the seabed. The pipe is welded on the deck of the lay vessel, passed over a stinger, and gradually lowered to the seabed. Although efficient for large-diameter pipelines, precise tension control is required to prevent excessive stress during installation [9].

J-lay Method

The J-lay method is well-suited for deepwater installations where the seabed is located at significant depths, making the S-lay method impractical. In this technique, the pipeline is deployed almost vertically from the vessel, forming a "J" shape as it reaches the seabed. This approach minimizes bending stress, making it particularly advantageous for deepwater projects. However, it is a slower method and necessitates the use of specialized vessels equipped with vertical lay towers and support structures [9].

Reel-lay Method

The reel-lay method involves spooling the pipeline onto a large reel aboard the vessel and unspooling it as the vessel progresses along the pipeline route. This technique enables rapid installation and is applicable to both shallow and deepwater operations. However, it is typically limited to smaller-diameter pipelines due to the internal stresses induced by the spooling process. The reel-lay method is particularly advantageous for projects requiring rapid deployment, such as tie-ins and short pipeline segments [9].

Table 2.1: Comparison of Pipeline Installation Methods

Method	Water Depth	Advantages	Challenges
S-lay	Shallow to moderate	Efficient for large-diameter pipelines	Requires precise stinger and tension control
J-lay	Deepwater	Reduces bending stress, suitable for extreme depths	Slower, requires specialized vessels
Reel-lay	Shallow and deep	Rapid installation	Limited to smaller-diameter pipelines

The selection of an installation technique depends on multiple factors, including water depth, pipeline diameter, and environmental conditions. A comprehensive understanding of these methods is essential for optimizing installation strategies in offshore projects [6].

2.3. Fundamental Principles in Subsea Hydrodynamics

The study of subsea hydrodynamics involves the interaction between fluid flow and submerged structures, governed by both linear and nonlinear dynamics. Fundamental principles, such as added mass, drag, and vortex-induced vibrations, are essential for understanding the forces acting on subsea installations [10]. Linear wave potential theory provides a foundation for approximating hydrodynamic forces in relatively calm sea states; however, it does not capture nonlinear effects that dominate under harsher conditions. Nonlinear phenomena, including wave drift forces and vortex shedding, require advanced computational methods to ensure accurate predictions. Morison's equation, a widely used semi-empirical approach, separates hydrodynamic forces into inertial and drag components based on Keulegan-Carpenter (KC) number regimes. However, its reliability decreases for structures exposed to significant wake interactions or irregular flow fields [13].

Recent advancements in Computational Fluid Dynamics (CFD) have addressed these limitations by solving the two- and three-dimensional Navier-Stokes equations under steady, unsteady, and transient flow conditions [1]. This approach enables the prediction of complex behaviors such as vortex shedding, boundary layer formation, turbulence intensity, and unsteady wake effects, which are critical for dynamic loads on subsea structures. Studies have validated the efficacy of CFD in modeling nonlinear hydrodynamic forces, particularly in applications requiring precision under higher sea states [14]. The integration of CFD tools with dynamic analysis software has further enhanced predictive accuracy in complex scenarios, such as installation under oscillatory flows [8, 23].

Key dimensionless parameters, including the Reynolds number and KC number, provide a framework for classifying flow regimes and determining the relative dominance of drag and inertial forces. Chakrabarti [23] highlights that the transition between laminar and turbulent flow regimes significantly influences the added mass and drag coefficients, underscoring the need for detailed parameterization in design and analysis. These principles form the foundation for understanding and optimizing subsea structures subjected to diverse environmental conditions [23].

2.3.1. Theoretical Background

Understanding the hydrodynamic forces acting on subsea structures requires a solid theoretical foundation. Two primary forces are of interest: **drag force** and **added mass force**. This section provides an overview of these forces and the fundamental principles governing them.

Drag Force

Drag force represents the resistance experienced by a body moving through a fluid or when a fluid flows around a stationary body. It depends on factors such as fluid viscosity, flow velocity, and the shape and surface roughness of the body [24]. The drag force F_D is given by:

$$F_D = \frac{1}{2} C_D \rho A u^2 \tag{2.1}$$

where:

- C_D is the drag coefficient,
- ρ is the fluid density,
- A is the reference area,
- u is the flow velocity relative to the body.

The drag coefficient C_D is influenced by the shape of the body and the Reynolds number, which characterizes the flow regime [25].

Added Mass Force

Added mass refers to the additional inertia a structure appears to possess when accelerating in a fluid, as it must displace a certain volume of surrounding fluid [26]. The added mass force F_A is expressed as:

$$F_A = C_A \rho V \dot{u} \tag{2.2}$$

where:

- C_A is the added mass coefficient,
- V is the displaced volume of the structure,
- $\dot{u}$ is the acceleration of the structure relative to the fluid.

The added mass coefficient C_A is dependent on the geometry of the structure and the flow conditions [27].

Morison's Equation

A significant development in hydrodynamic analysis is Morison's equation, introduced by Morison et al. [13]. This empirical equation is used to calculate the hydrodynamic forces acting on slender, cylindrical structures by separating the total force into drag and inertial components. For a cylindrical structure with diameter D, subjected to flow velocity u and acceleration $\dot{u}$, the in-line hydrodynamic forces per unit length are given by:

$$F = C_m \cdot \rho \cdot \pi \cdot \frac{D^2}{4} \cdot \dot{u} + C_d \cdot \rho \cdot \frac{D}{2} \cdot u \cdot |u| \tag{2.3}$$

where:

- F: Total in-line hydrodynamic force per unit length $[N/m]$,
- C_m: Inertia coefficient, representing the added mass effect due to water acceleration around the structure,
- C_d: Drag coefficient, representing resistance from viscous forces as water flows past the structure,

- ρ: Density of seawater $[kg/m]$, typically 1025 kg/m^3,
- D: Diameter of the cylindrical structure $[m]$,
- $\dot{u}$: Flow acceleration $[m/s]$, contributing to inertial forces,
- u: Flow velocity $[m/s]$, contributing to drag forces,
- $|u|$: Absolute value of flow velocity $[m/s]$, indicating the directionality of the drag force.

Morison's equation is particularly effective for slender structures in comparison to the wavelength of waves, such as risers and pipelines during installation. Its validity is influenced by factors including structural slenderness, wave force periodicity, and the appropriate application of linearized drag forces.

2.3.2. Flow Conditions and Their Impact on Hydrodynamic Forces

The surrounding flow conditions significantly influence the behavior of submerged structures in offshore environments. External flow past submerged objects generates various fluid dynamic conditions that dictate the magnitude and nature of hydrodynamic forces. The application of traditional hydrodynamic models, such as Morison's equation, is generally effective for simple geometrical structures like squares, cylinders, and cubes, where flow interactions remain relatively predictable. However, for more complex geometries—such as Pipeline End Terminations (PLETs), Pipeline End Manifolds (PLEMs), mudmats, and roller guide structures—the flow dynamics become highly intricate. These structures introduce additional members, varying cross-sectional areas, and sharp edges, leading to flow separation, vortex shedding, and diffraction effects.

Non-streamlined bodies with large surface areas perpendicular to flow experience increased turbulence, higher drag forces, and complex pressure distributions. In contrast, streamlined bodies minimize flow resistance, reducing turbulence and ensuring more predictable hydrodynamic forces. The irregular and often turbulent nature of these flow conditions necessitates advanced modeling techniques for accurate force predictions. Computational Fluid Dynamics (CFD) has become an indispensable tool in offshore engineering, enabling detailed simulations of fluid-structure interactions and capturing the nuances of flow behavior around complex geometries.

Figure 2.4 illustrates the interaction of fluid flow with streamlined bodies, highlighting differences in flow behavior between streamlined and non-streamlined geometries.

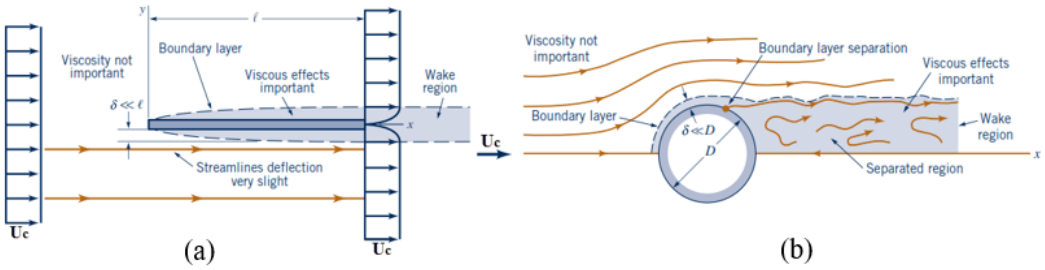

Figure 2.4: Fluid-structure interaction for streamlined bodies in the flow direction [28].

2.4. Hydrodynamic Load Modeling Methods

Traditionally, the industry has relied on methodologies prescribed by standards such as Det Norske Veritas (DNV). Recent advancements in Computational Fluid Dynamics (CFD) offer a promising alternative, providing more detailed and accurate hydrodynamic load predictions [29, 30].

1. DNV Methods: The DNV standards, such as DNV-RP-C205 [31], provide empirical formulas and guidelines for estimating hydrodynamic loads. These methods typically employ Morison's equation, which combines inertia and drag forces to predict loads on slender structures such as pipelines and risers. The formula is computationally efficient and practical for engineering applications. However, DNV methods rely on empirical coefficients derived from experimental data and potential flow Boundary Element Method (BEM) models, which assume inviscid, incompressible, and irrotational flow. Consequently, complex flow interactions may not be fully captured [8, 6].

2. Computational Fluid Dynamics (CFD): CFD numerically solves the two- and three-dimensional Navier-Stokes equations to simulate fluid flow around structures. This approach models intricate fluid-structure interactions, capturing effects such as vortex shedding, turbulence, and wake formation. CFD simulations offer higher accuracy, particularly for irregular geometries and varying flow conditions. However, the computational cost is significantly higher, and expertise is required for setup, validation, and interpretation of results [32].

Table 2.2: Comparison of DNV Methods and CFD

Aspect	DNV	CFD
Accuracy	Simplified empirical formulas; less detailed.	High accuracy; captures complex interactions.
Computational Resources	Low; suitable for quick assessments.	High; requires significant computational power.
Reliability	Well-validated; widely used in the industry.	Requires case-specific validation.
Application Scope	Best suited for standard, uniform scenarios.	Ideal for complex, non-uniform geometries.
Integration	Limited integration with advanced tools.	Easily integrated with dynamic simulations (e.g., OrcaFlex).

2.5. CFD Theory and Applications

2.5.1. Theoretical Foundations

Computational Fluid Dynamics (CFD) is a specialized domain within fluid mechanics that employs numerical techniques to analyze fluid flow phenomena. The fundamental principles of CFD are based on the Navier-Stokes equations, which encapsulate the conservation laws of mass, momentum, and energy within a fluid system [16].

Navier-Stokes Equations

The Navier-Stokes equations describe the fundamental principles governing fluid motion. These equations are derived from the conservation laws of mass, momentum, and energy.

Continuity Equation (Mass Conservation) The continuity equation ensures mass conservation within the fluid domain:

$$\frac{\partial \rho}{\partial t} + \nabla \cdot (\rho \mathbf{u}) = 0 \tag{2.4}$$

where:

- ρ is the fluid density ($\mathrm{kg/m^3}$),
- $\mathbf{u} = (u, v, w)$ is the velocity vector, with components in the x, y, and z directions ($\mathrm{m/s}$),
- $\nabla \cdot (\rho \mathbf{u})$ represents the divergence of mass flux.

This equation states that any change in fluid density within a control volume is balanced by the net mass flux through the control volume's boundaries.

Momentum Equation (Momentum Conservation) The momentum equation accounts for changes in fluid momentum due to pressure gradients, viscous effects, and body forces:

$$\frac{\partial(\rho \mathbf{u})}{\partial t} + \nabla \cdot (\rho \mathbf{u}\mathbf{u}) = -\nabla p + \nabla \cdot \boldsymbol{\tau} + \mathbf{f} \tag{2.5}$$

where:

- $\rho \mathbf{u}$ is the momentum per unit volume ($\mathrm{kg/(m^2 s)}$),
- $\frac{\partial(\rho \mathbf{u})}{\partial t}$ represents the local acceleration term (rate of change of momentum),
- $\nabla \cdot (\rho \mathbf{u}\mathbf{u})$ is the convective acceleration (momentum transport by the fluid motion),
- p is the pressure field (Pa),
- $\boldsymbol{\tau}$ is the viscous stress tensor, which accounts for internal friction due to fluid viscosity,
- $\mathbf{f}$ represents external body forces, such as gravitational or buoyancy forces.

In expanded form for an incompressible Newtonian fluid, the stress tensor is given by:

$$\boldsymbol{\tau} = \mu \left[\nabla \mathbf{u} + (\nabla \mathbf{u})^T \right] - \frac{2}{3} \mu (\nabla \cdot \mathbf{u}) \mathbf{I} \tag{2.6}$$

where:

- μ is the dynamic viscosity of the fluid ($\mathrm{Pa \cdot s}$),
- $\mathbf{I}$ is the identity matrix.

This equation describes how velocity gradients within the fluid contribute to internal stresses.

Energy Equation (Energy Conservation) The energy equation accounts for internal energy, kinetic energy, and heat transfer:

$$\frac{\partial(\rho E)}{\partial t} + \nabla \cdot (\rho E \mathbf{u}) = -\nabla \cdot \mathbf{q} + \boldsymbol{\tau} : \nabla \mathbf{u} + q_{\text{ext}} \tag{2.7}$$

where:

- E is the total energy per unit mass, defined as:

$$E = e + \frac{1}{2} |\mathbf{u}|^2 \tag{2.8}$$

- e is the internal energy per unit mass ($\mathrm{J/kg}$),
- $\frac{1}{2} |\mathbf{u}|^2$ represents the kinetic energy per unit mass,

- $\nabla \cdot \mathbf{q}$ is the divergence of the heat flux vector, governed by Fourier's law of heat conduction:

$$\mathbf{q} = -k\nabla T \tag{2.9}$$

  where k is the thermal conductivity (W/(m·K)) and T is the temperature (K),

- $\boldsymbol{\tau} : \nabla \mathbf{u}$ accounts for viscous dissipation,
- q_{ext} represents external heat sources or sinks.

This equation describes how the total energy of a fluid element changes due to convection, conduction, work done by pressure and viscous forces, and external heat addition.

The Navier-Stokes equations form the foundation for CFD modeling, governing fluid flow under various conditions. These equations must be solved numerically for complex flow problems, as analytical solutions are only feasible for simple cases. In this research, these equations were discretized using the finite volume method (FVM) and solved within the CFD framework to obtain hydrodynamic in line and perpendicular forces to the induced flow on subsea structures.

Further details on governing equations, discretization methods, and turbulence modeling are discussed in Appendix A.

2.6. CFD Workflow and Modeling

The CFD process consists of several key steps, ensuring systematic simulation from geometry modeling to post-processing [30, 15].

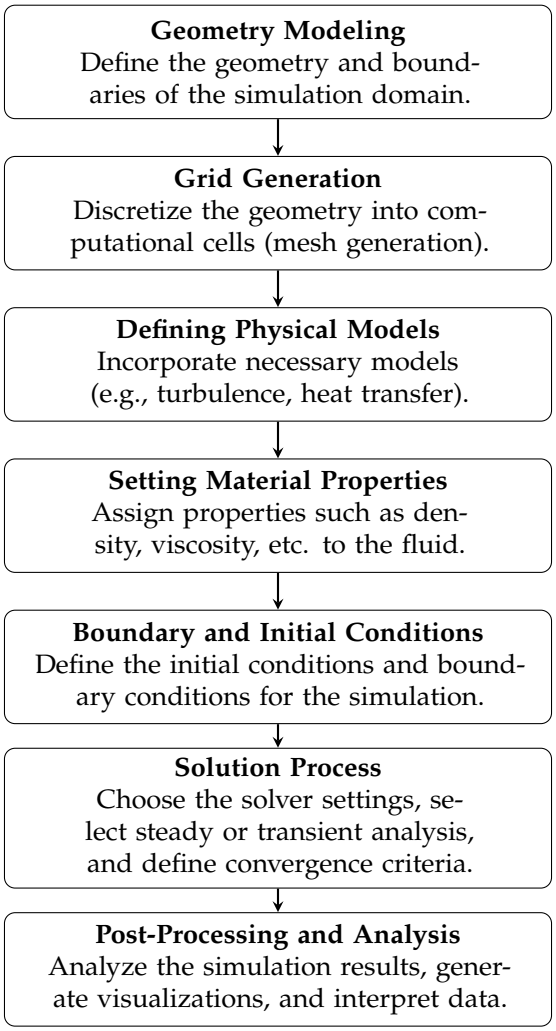

Figure 2.5: General Workflow for CFD Simulation[29]

2.6.1. CFD Modelling using STAR-CCM+

As outlined in section 1.2, the increasing scale of subsea structures has led to heightened complexity in hydrodynamic load modelling challenges. Geometric intricacies, such as sharp edges and auxiliary components, amplify difficulties in accurately predicting flow behavior, particularly under accelerated flow conditions. Computational Fluid Dynamics (CFD) simulations, including model-scale experiments, remain critical for resolving these challenges and to investigate flow induced motions. [29].

STAR-CCM+, a commercial CFD software widely adopted in marine technology, is employed for simulating multiphase flows and hydrodynamic loads on structures. Its capabilities in free-surface modeling and transient flow analysis make it suitable for subsea applications. The workflow comprises three phases: preprocessing, simulation, and post-processing [15].

Preprocessing Phase

The preprocessing phase involves defining simulation parameters and domain geometry. Key decisions include steady/unsteady flow, internal/external flow, and 2D/3D dimensionality. A rigid, enclosed geometry is modeled in parametric Computer-Aided Design (CAD) format to minimize flow disturbances caused by sharp edges.

A sufficiently large fluid domain is constructed to avoid boundary interference. Domain size directly influences computational cost due to increased mesh resolution requirements. Fluid properties (e.g., density, viscosity) and operational parameters (e.g., gravity) are assigned based on the simulated scenario. Geometry segmentation is applied to optimize boundary condition application and computational efficiency.

Mesh generation employs structured or unstructured discretization schemes. Grid resolution is intensified in regions of anticipated high velocity or pressure gradients (e.g., near walls, wakes). For 3D simulations, refinement zones and non-conformal meshing are implemented to capture flow characteristics while minimizing cell count. Mesh independence is verified by comparing results across progressively refined grids.

Solver Settings

The solver phase configures physical models and numerical parameters. Turbulence models (e.g., k-ϵ, k-ω, LES, DES) are selected based on flow regime and accuracy requirements [29]. Boundary conditions prescribe inlet velocity, outlet pressure, and wall interactions (no-slip, symmetry).

Steady-state simulations employ implicit solvers with second-order spatial discretization, while transient analyses use bounded temporal schemes. Convergence criteria (e.g., residual thresholds below 10^{-5}) and iteration limits are defined. Solution stability is monitored via force coefficients and residuals for mass/momentum equations.

Post-Processing Phase

Post-processing extracts quantitative and qualitative results from converged simulations. Contour plots visualize pressure/velocity distributions, while streamlines identify recirculation zones and flow separation. Force coefficients (drag C_d, lift C_l) are computed using surface integrals of pressure and shear stresses.

Validation against experimental data or analytical solutions verifies model accuracy. Discrepancies exceeding 10% trigger mesh refinement or turbulence model reassessment. Processed data is exported for comparative analysis in engineering reports.

Limitations

While STAR-CCM+ excels in hydrodynamic simulations, three limitations arise in subsea installation modeling:

- Overset grid interpolation errors during large structural motions, leading to unsteady force inaccuracies [33].
- High computational costs of LES/DES turbulence models for fine-mesh 3D simulations.
- Interface smearing in multiphase flows, affecting wave-structure interaction fidelity.

These constraints necessitate trade-offs between accuracy and computational feasibility for industrial applications.

3

Literature Review

3.1. Introduction

A comprehensive examination of previous research efforts is essential for understanding hydrodynamic loads acting on subsea structures. Accurate prediction of these loads is critical due to the complex nature of fluid dynamics, where both overestimation and underestimation can significantly impact engineering applications, particularly in design safety and operational efficiency. This chapter reviews the methodologies employed to analyze and predict hydrodynamic interactions with subsea structures, encompassing analytical, experimental, and numerical approaches. By critically evaluating these methods, the strengths and limitations of each approach are identified, providing a foundation for the advanced methodologies implemented in subsequent sections of this thesis.

The chapter is structured as follows:

- **Analytical Studies:** A review of theoretical approaches, including empirical formulas and semi-analytical models, with an emphasis on their applicability and limitations.
- **Experimental Studies:** An examination of experimental approaches, their role in validating theoretical models, and the insights they provide into hydrodynamic behavior.
- **Numerical Studies:** An evaluation of numerical methods, particularly Computational Fluid Dynamics (CFD), highlighting their capability to capture complex fluid-structure interactions.
- **Critical Analysis:** A comparative assessment of the reviewed methods, identifying research gaps and challenges in hydrodynamic load prediction.
- **Research Gaps and Questions:** Identification of key research gaps and formulation of research questions that guide the thesis.

This chapter aims to synthesize existing studies and knowledge, leading to the identification of research gaps and the development of research questions. These gaps will be addressed through CFD modeling and analysis in the subsequent chapters.

3.2. Analytical Studies

Analytical approaches have historically provided fundamental insights into hydrodynamic load prediction for subsea structures. These methods primarily rely on simplified theoretical models and empirical formulas to approximate fluid-structure interactions. While invaluable for preliminary design assessments and rapid estimations, their accuracy is constrained by the assumptions of potential flow theory and linear wave theory, which may not fully capture the complexities of real-world subsea environments.

Empirical formulas, such as those derived from Morison's equation, offer a straightforward means of calculating drag and inertia forces, particularly for cylindrical structures such as piles and risers. Morison's equation, initially developed for slender bodies, combines inertia and drag components to estimate the total force acting on a structure. This approach has been widely adopted in offshore engineering due to its simplicity and computational efficiency. However, its applicability is limited by the assumptions of linear wave theory and laminar flow conditions, which can introduce inaccuracies in turbulent or complex flow scenarios [25].

Mavrakos et al. [34] conducted a seminal research on the linearized hydrodynamic radiation problem for concentric, free-surface-piercing truncated vertical cylinders using the Galerkin method. Their findings underscored the significant impact of added mass and damping forces, particularly under resonance conditions, where phenomena such as negative added mass were observed. These insights are critical for optimizing subsea designs, especially in mitigating resonant responses during operation [27].

Semi-Analytical Models

Semi-analytical models serve as an intermediary between purely empirical formulas and computationally intensive numerical methods. These models incorporate empirical data, potential flow theory, and numerical correction factors to estimate hydrodynamic coefficients. Early contributions by Peterson [35] and Humphreys [36] established the use of potential flow solutions combined with empirical adjustments for underwater vehicle design. Subsequent advancements by Maeda [**maeda1988research**] and Nahon [37] introduced refinements to these methods by integrating data from towing tank tests and rotating arm mechanisms to better capture the dynamic behavior of submerged structures.

Geisbert [38] expanded on these methods by applying semi-empirical techniques to estimate hydrodynamic coefficients for Autonomous Underwater Vehicles (AUVs). These models combined empirical drag coefficients with theoretical added mass predictions, achieving improved accuracy over purely analytical approaches. More recent studies by Isa [39], have refined these models further using hybrid methodologies that incorporate numerical simulations to correct and validate empirical data, enhancing their applicability to a broader range of geometries and range of flow conditions.

Limitations and Applicability

Although analytical and semi-analytical methods provide valuable initial insights, their reliance on idealized conditions limits their accuracy in complex offshore environments. These methods are most effective in early-stage design evaluations or as supplementary tools alongside more robust numerical approaches. Their primary limitations stem from assumptions of linearity, small-amplitude motions, and potential flow, which may not adequately account for nonlinear effects, flow separation, or the presence of intricate geometrical features.

The following sections will examine experimental and numerical methods, which address these limitations by providing direct measurements and detailed simulations of hydrodynamic forces. The

integration of these methods into a cohesive framework for predicting hydrodynamic loads on subsea structures will be explored, emphasizing the necessity of a multi-faceted approach to accurately capture fluid-structure interactions in offshore engineering.

3.3. Experimental Studies

Extensive research has been conducted to accurately estimate added mass and drag coefficients for subsea structures.[40, 14, 41, 42, 43, 44, 45]. This section reviews key experimental studies that have contributed to understanding the fundamental characteristics of these coefficients under both steady and oscillatory flow conditions.

Keulegan and Carpenter's seminal work established the relationship between drag and inertia forces in oscillatory flows. The introduction of the Keulegan-Carpenter (KC) number enabled characterization of the relative importance of drag and inertia forces acting on submerged structures. Their experiments demonstrated that for low KC numbers, the flow is inertia-dominated, whereas for high KC numbers, drag forces become more significant. The KC number is defined as:

$$KC = \frac{U_m T}{D} \tag{3.1}$$

Also, their research explored the influence of the Reynolds number Re on drag and inertia coefficients, revealing that an increase in Reynolds number results in a decrease in the drag coefficient, indicating a transition from laminar to turbulent flow [46].

Sarpkaya conducted extensive experimental research in the 1970s and 1980s, further advancing the understanding of hydrodynamic forces in oscillatory flows. Empirical correlations for drag and inertia coefficients were developed as functions of the KC number and Reynolds number. His findings demonstrated a nonlinear relationship between the drag coefficient and the KC number, which is critical for accurately predicting forces in oscillatory flows [44, 47]. Furthermore, Sarpkaya investigated the impact of surface roughness on drag coefficients, revealing that increased roughness leads to higher drag forces, particularly in turbulent flow regimes. These insights are essential for subsea structure design, where surface conditions significantly influence hydrodynamic loading [47].

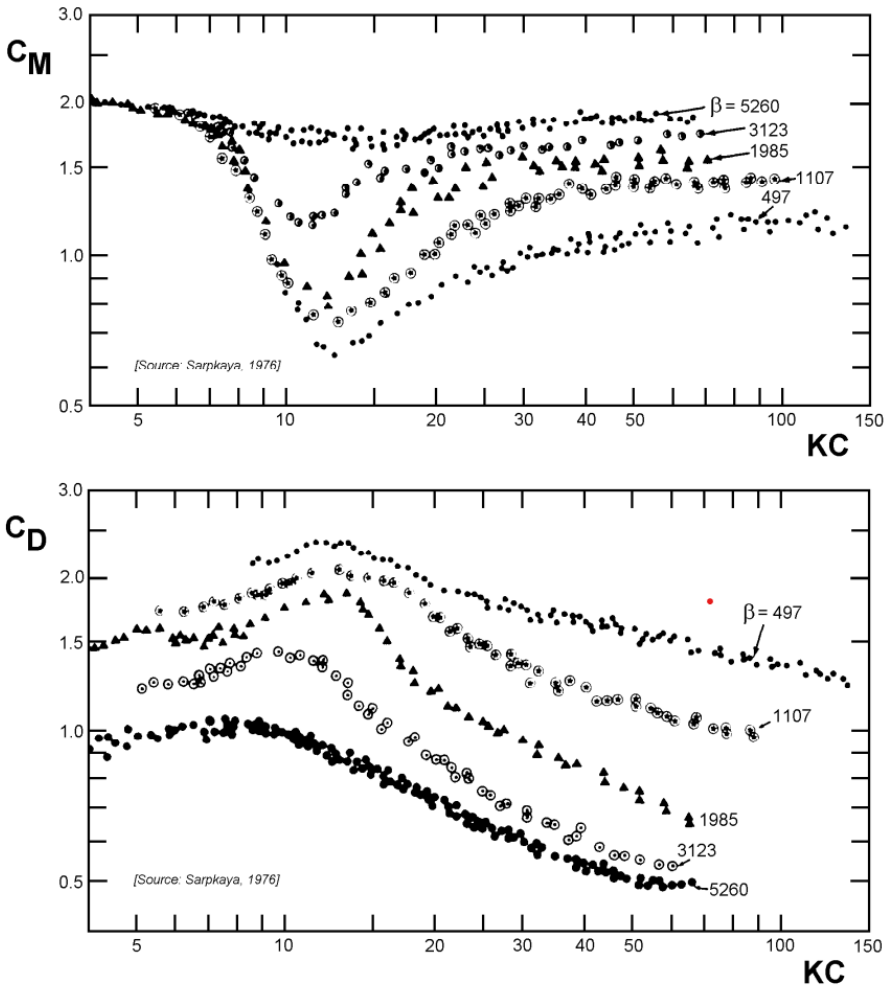

Figure 3.1: Variation of drag and inertia coefficients with KC number from Sarpkaya's experiments [44].

An et al. [48] investigated the forced harmonic heave motion of horizontally submerged and perforated rectangular plates under varying submergence conditions. Both experimental and numerical methods were utilized to decompose hydrodynamic loads into coefficients for analysis. The numerical approach integrated potential flow theory, linear free surface conditions, and a nonlinear viscous pressure loss condition. The Boundary Element Method (BEM) was employed for the inner domain, while empirical techniques were used for velocity potentials in the outer domain. Their results demonstrated strong agreement between numerically estimated heave-added mass and damping coefficients and experimental values, emphasizing the KC number's linear dependency on hydrodynamic coefficients across different submergence conditions.

Bunnik [49] conducted experiments focusing on wave loads, added mass, drag, and structural damping, particularly in the splash zone, where wave-induced effects lead to significant structural motions. Two primary types of tests were performed:

- **Decay Tests:** Utilized to estimate added mass and damping coefficients.
- **Captive Tests:** Conducted to evaluate wave loads from incoming regular waves.

These tests analyzed structures at various orientations and depths, including fully submerged and

near-seabed conditions, providing insight into the variability of hydrodynamic forces under different submersion scenarios.

Li et al. [42] investigated the hydrodynamic coefficients of heave plates used in Spar platforms, specifically analyzing their response to heave motion. Forced oscillation tests were performed to assess the effects of parameters such as the KC number, oscillation frequency, depth, thickness-to-width ratio, perforation factor, and hole size on hydrodynamic coefficients. Both single-plate and multiple-plate configurations were tested, demonstrating the influence of structural configuration on Spar platform response.

Nam et al. [41] examined the coupled motion responses between a floating crane vessel and a lifted subsea manifold during deep-water installations. Both experimental and numerical approaches were employed to assess the effects of perforation percentages and dynamic tension variations in hoisting wires under different wave conditions. The research also evaluated the impact of passive heave compensators on motion and tension responses, underscoring the significance of coupled dynamics in subsea structure installation.

Experimental studies play a crucial role in validating numerical models and improving the understanding of hydrodynamic coefficients across a range of flow conditions. These studies provide empirical data essential for refining numerical simulations, particularly in capturing complex interactions between waves, currents, and submerged structures in marine environments. The insights gained from these experiments contribute to the accuracy of hydrodynamic load predictions, ultimately enhancing the safety and efficiency of subsea installations.

3.4. Numerical Studies

Numerical methods, particularly Computational Fluid Dynamics (CFD), are essential for predicting hydrodynamic forces on subsea structures due to their ability to model complex fluid-structure interactions. This section examines key numerical studies, emphasizing advancements, methodologies, and validation efforts in estimating hydrodynamic coefficients for various submerged and subsea structures.

Significant progress has been made in numerical simulations, enabling detailed investigations of hydrodynamic coefficients through techniques such as steady and unsteady Reynolds-Averaged Navier-Stokes (RANS) simulations. These methods have been employed to replicate conditions found in experimental setups, such as towing tanks and rotating arm tests. For instance, Li et al. [50] conducted RANS simulations to estimate hydrodynamic coefficients for submerged rotating propellers, revealing that these coefficients exhibit a linear dependency on the ratio of oscillation frequency to blade passing frequency, providing insights into the dynamic behavior of such rotating bodies.

Case research: Hydrodynamic Coefficients of Subsea Manifolds

Du et al. [14] investigated the hydrodynamic coefficients of subsea manifolds using both CFD and experimental model testing. Their findings indicated that the drag coefficients obtained from CFD simulations closely matched experimental values, confirming the reliability of numerical methods. Additionally, results demonstrated a linear relationship between the added mass coefficients and the Keulegan-Carpenter (KC) number, with minimal influence from oscillation frequency, which is critical for predicting the dynamic response during subsea installations.

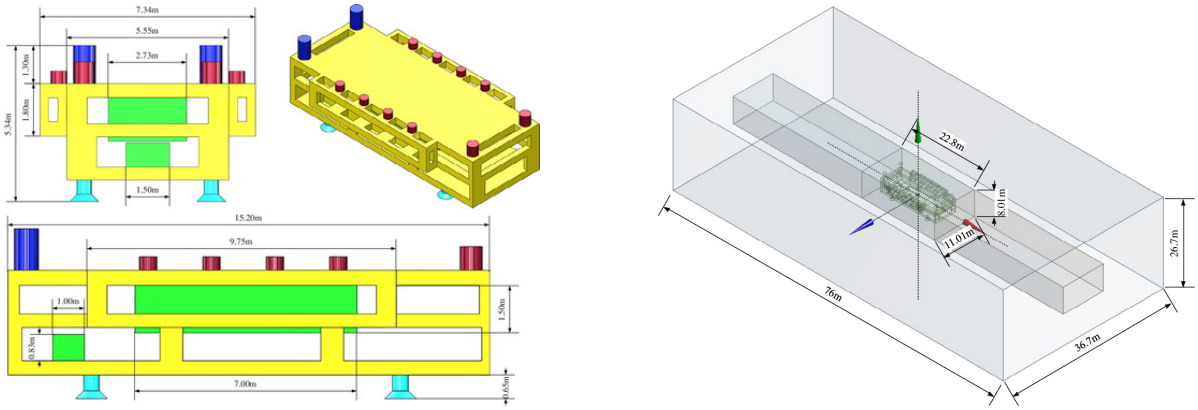

(a) Simplified subsea manifold model used in CFD simulations.

(b) Numerical domain setup for CFD analysis [14].

Figure 3.2: Numerical geometry and domain setup.

Validation and Comparison with Experimental Data

Validation of CFD results is essential for establishing their accuracy and reliability. Pan et al. [51] utilized RANS simulations alongside Physical Model Motion (PMM) experiments to predict the hydrodynamic coefficients of an underwater submarine, demonstrating strong agreement between numerical and experimental results. Similarly, Gadelho et al. [52] applied CFD to evaluate ship hull sections under heave and sway motions in shallow and deep waters. The CFD results closely aligned with potential flow theory, except in regions with significant vortex formation, highlighting the necessity of accounting for viscous effects in simulations.

Despite the detailed insights provided by CFD, challenges remain, particularly in mesh generation and solver accuracy. Reddy et al. [53] observed variations in drag predictions due to inadequate mesh resolution and improper boundary condition setups. These findings underscore the necessity for meticulous meshing strategies and robust validation protocols to ensure the reliability of CFD predictions in complex flow environments.

Hybrid Approaches Combining Numerical and Experimental Methods

The integration of numerical simulations with experimental data enhances the robustness of hydrodynamic coefficient estimations. Liang et al. [43] combined CFD simulations with towing tank tests to research the drag coefficients of subsea trees. This hybrid approach allowed for the validation of CFD results against experimental observations, providing a comprehensive understanding of the hydrodynamic behavior of complex geometries under various flow conditions.

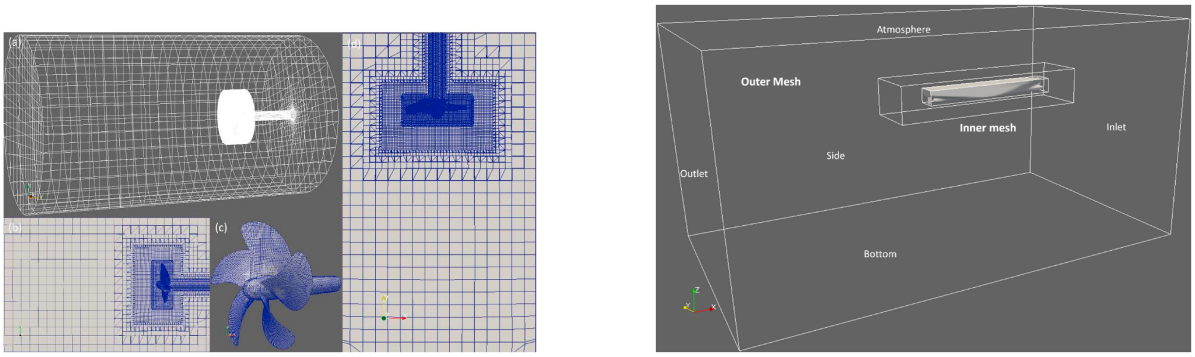

(a) Overset mesh technique used in CFD simulations.

(b) Boundary condition setup in CFD simulations.

Figure 3.3: Meshing strategies and boundary conditions [52].

Numerical methods, particularly CFD, have significantly advanced the understanding and prediction of hydrodynamic coefficients for subsea structures. By integrating numerical simulations with experimental data, these studies offer comprehensive insights into fluid-structure interactions, supporting the optimization of offshore installations. The combined use of CFD and traditional validation methods provides a robust framework for accurately estimating hydrodynamic forces under diverse marine conditions [14, 54, 32].

This section provides an overview of key research articles that have contributed to the understanding and estimation of hydrodynamic coefficients for subsea structures. The review encompasses both general studies on hydrodynamic loading and investigations into specific submerged and subsea geometries, focusing on the methodologies employed and their findings. A comprehensive list of reviewed articles is provided in Appendix B.

As discussed in chapter 1 the accurate estimation of hydrodynamic coefficients, including drag and inertia coefficients, is essential for predicting the dynamic response of submerged structures in marine environments. This section presents a comparative analysis of methodologies used for estimating these coefficients, encompassing empirical, analytical, experimental, and numerical approaches. The advantages and limitations of each method are discussed in Appendix section B.1, providing a robust understanding of their applicability.

3.5. Limitations and Research Gaps

This section critically evaluates prior research on hydrodynamic coefficient estimation, focusing on added mass and damping effects, which significantly influence the forces and moments acting on subsea structures. Various empirical, analytical, experimental, numerical, and hybrid methodologies are examined, highlighting their advantages and inherent limitations.

Empirical and Analytical Methods

Empirical methods provide rapid estimates of hydrodynamic coefficients using established correlations derived from experimental data. While widely employed due to their simplicity, their applicability is limited to conditions similar to those in the original datasets. Analytical methods offer fundamental insights into fluid-structure interactions by solving idealized theoretical models. However, their reliance on assumptions such as potential flow and ideal boundary conditions restricts their accuracy when applied to complex subsea environments.

Experimental Approaches

Experimental methods provide direct measurements of hydrodynamic forces under controlled conditions, serving as essential validation tools for theoretical and numerical models. Despite their high reliability, these methods are constrained by significant costs, time requirements, and challenges associated with replicating full-scale marine conditions. Notable studies, such as Mentzoni et al. [55], examined the hydrodynamic coefficients of simplified subsea structures using flume experiments. Their findings indicated that vertical hydrodynamic forces exceeded horizontal forces and that wave-induced vortex shedding significantly influenced structural responses.

Numerical Methods: CFD Applications

Computational Fluid Dynamics (CFD) has gained prominence for hydrodynamic coefficient estimation due to its ability to model complex fluid-structure interactions with high precision. CFD facilitates detailed analysis of flow fields and force distributions around submerged structures, yielding insights that are often difficult to obtain experimentally. Xiang et al. [56] demonstrated the effectiveness of CFD in predicting hydrodynamic coefficients for an inclined prism near the seabed, revealing significant dependencies on shallow water depths and varying bathymetry.

Despite its advantages, CFD is computationally intensive and requires expertise in meshing strategies, solver selection, and boundary condition specification. The sensitivity of CFD results to mesh quality was highlighted by Reddy et al. [53], who underscored the importance of proper meshing techniques and rigorous validation against experimental data. While these challenges persist, CFD remains an indispensable tool for simulating steady and unsteady hydrodynamic behavior in offshore applications.

Hybrid Approaches and Comparative Studies

Hybrid methodologies, combining numerical simulations with experimental data, enhance the robustness of hydrodynamic coefficient estimations. Liang et al. [43] conducted towing tank tests and CFD simulations to investigate drag forces on subsea trees, demonstrating that an integrated approach provided a more comprehensive understanding of hydrodynamic behavior across various flow conditions.

Comparative studies, such as those by Venugopal et al. [57], highlight the discrepancies between different estimation techniques and emphasize the necessity of selecting an appropriate approach based on specific project requirements. While empirical and analytical methods offer quick estimates, CFD provides highly detailed predictions, albeit at a greater computational cost. The selection of a suitable methodology must consider structural complexity, environmental conditions, and accuracy requirements. A summary of key studies on hydrodynamic coefficients and forces is provided in Table B.6, outlining their objectives, methodologies, and major findings. This comparative analysis underscores the diversity of approaches and the continued need for enhanced predictive capabilities in subsea hydrodynamics.

Existing literature reveals significant limitations in traditional hydrodynamic load prediction methods for complex subsea structures under high sea states [58]. CFD has emerged as a promising alternative due to its ability to model intricate geometries and capture nonlinear effects [59]. Li et al. [59] demonstrated that CFD simulations accurately captured vortex-induced vibrations and hydrodynamic forces on subsea pipelines, outperforming traditional methods.

However, three primary challenges and gaps hinder the widespread adoption of CFD:

- **Validation of CFD Models:** Comprehensive validation of CFD models for complex subsea structures, such as the J-lay PLET under high sea states, remains limited. Without validation against experimental data, uncertainties persist regarding the predictive reliability of CFD models [30].
- **Integration with Dynamic Simulations:** Incorporating CFD-derived hydrodynamic coefficients into dynamic simulation tools used for offshore installation analysis, such as OrcaFlex, presents integration challenges. Differences in data formats, modeling methodologies, and the need for coupled fluid-structure interaction modeling complicate effective implementation [14].
- **Comparative Studies:** Few studies have systematically compared CFD predictions with traditional empirical and analytical methods. A lack of comparative analysis hinders the demonstration of CFD's practical advantages for industry applications [60].

These research gaps align with the objectives outlined in section 1.3 and fall within the scope defined in section 1.4.

3.6. Formulation of Research Questions

To address the identified research gaps, the following main research question and sub-research questions are formulated:

Main Research Question:

Can CFD-based models improve hydrodynamic load predictions for a J-lay Pipeline End Terminal (PLET) installation under higher sea states, enhancing workability?

Sub-Research Questions:

1. **Validation of CFD Models:** Can the developed 2D CFD models accurately predict drag and added mass coefficients for thin flat plates when validated against experimental data?
2. **Extension to Full-Scale Simplified Structures:** How can CFD models of simplified full-scale structures (mudmat, folded mudmat, roller guides) be developed to predict hydrodynamic drag coefficients under high sea states relevant to J-lay PLET installations?
3. **Comparison with Traditional Methods:** How do the hydrodynamic coefficients (C_D and C_A) obtained from CFD simulations of simplified full-scale structures compare with DNV guidelines?
4. **Impact on Dynamic Installation Simulations:** Does the use of CFD-derived hydrodynamic coefficients in dynamic installation simulations lead to changes in predicted bending strains in sagbend compared to those using DNV coefficients, thereby improving workability?

These sub-research questions focus on validating CFD models, extending them to full-scale structures, performing comparative analyses, and assessing their impact on dynamic installation simulations.

This literature review has identified the limitations of traditional methods in predicting hydrodynamic forces on complex subsea structures and has underscored the potential of CFD in addressing these limitations. The critical analysis highlighted key challenges, including the need for validated CFD models, the development of full-scale simplified models, a lack of comparative studies with traditional methods, and the integration of CFD-derived coefficients into dynamic simulations. The next chapter outlines the methodology used to develop and validate CFD models, perform comparative analyses, and incorporate CFD-derived hydrodynamic coefficients into dynamic installation simulations.

4

Methodology

This chapter presents the methodologies used to develop and validate Computational Fluid Dynamics (CFD) simulations for predicting hydrodynamic loads on subsea structures. CFD provides a powerful tool for analyzing complex offshore fluid-structure interactions that are challenging to capture experimentally or through simplified analytical methods [61, 62]. An overview of the research framework is illustrated in Figure 4.1, guiding through each methodological step, from initial model development and validation under simplified conditions to full-scale, three-dimensional (3D) dynamic installation analyses.

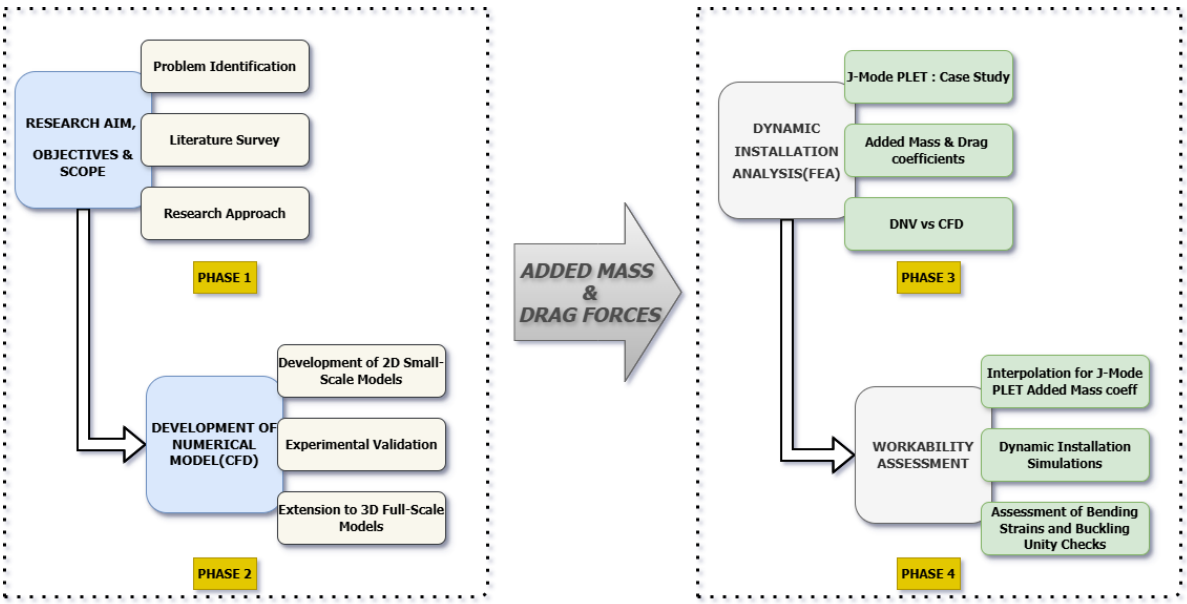

Figure 4.1: Overview of the research framework

4.1. Development of CFD Models

CFD simulations solve the Navier-Stokes equations, capturing the conservation of mass and momentum in fluid flow and enabling the resolution of fully 3D velocity fields, vortex shedding, and boundary

layer effects [16, 63]. Both k-ϵ and k-ω SST turbulence models were employed. The k-ϵ model was often chosen for its computational efficiency in steady external flows [61, 64], while the k-ω SST model provides enhanced accuracy in capturing flow separation and near-wall phenomena [65], essential for oscillatory and 3D scenarios.

High-quality meshes refined near structure surfaces were generated to accurately resolve boundary layers and wake dynamics [62]. Mesh independence studies ensured that results did not change significantly with further refinement (less than 1% variation in force coefficients). Boundary conditions reflected offshore environments, including uniform steady currents and oscillatory wave-induced flows [66, 67]. Fluid properties were chosen to represent seawater with a density of approximately $1030\,\mathrm{kg/m^3}$ and a dynamic viscosity of $8.8871 \times 10^{-4}\,\mathrm{Pa \cdot s}$.

Model validation was achieved by comparing numerical results against experimental data and established benchmarks [63]. After initial validation in 2D steady and oscillatory conditions, the methodology progressed to full-scale, 3D simulations to capture complex spatial flow structures, aspect ratio effects, and detailed hydrodynamic load distributions [62, 64].

Finally, CFD-derived forces and added mass coefficients were integrated into a dynamic finite element analysis (FEA) of a J-Mode Pipeline End Terminal (PLET) installation under realistic sea states. This approach addressed the research questions defined in the literature review, ensuring that the chosen models and scaling strategies were both scientifically robust and practically relevant.

4.1.1. Steady Flow Simulations

Steady flow simulations were first conducted to validate the CFD approach using a canonical test case: a thin flat plate ($0.1\,\mathrm{m} \times 0.1\,\mathrm{m} \times 0.003\,\mathrm{m}$) exposed to uniform currents. The fluid density was initially set to $1000\,\mathrm{kg/m^3}$ to match standard test conditions [63]. The computational domain was extended sufficiently to minimize boundary effects. A typical domain extended approximately 2 m upstream, 1.25 m on each side, and 2 m downstream of the plate. This domain size was determined via sensitivity analyses, ensuring negligible influence of boundaries on the flow around the plate.

An unstructured mesh was employed (see Figure 4.2), with refinement near the plate surface to accurately resolve boundary layers. The k-ϵ turbulence model was chosen for its robustness and computational efficiency. Residuals for velocity, pressure, and turbulence quantities were monitored until they fell below 10^{-6}, ensuring convergence.

Velocities of 1 to 3 m/s were tested to cover a range of Reynolds numbers representative of subsea currents [31]. Resulting velocity fields and wake formations were compared with published experimental data [63], confirming the reliability of the numerical approach.

Table 4.1: Boundary conditions for steady flow simulations, emulating uniform subsea currents interacting with a stationary plate.

Boundary	Condition
Inlet	Uniform velocity inlet (u = 1–3 m/s)
Outlet	Zero-gauge pressure outlet
Plate Surface	No-slip wall
Domain Walls	Symmetry or far-field boundary

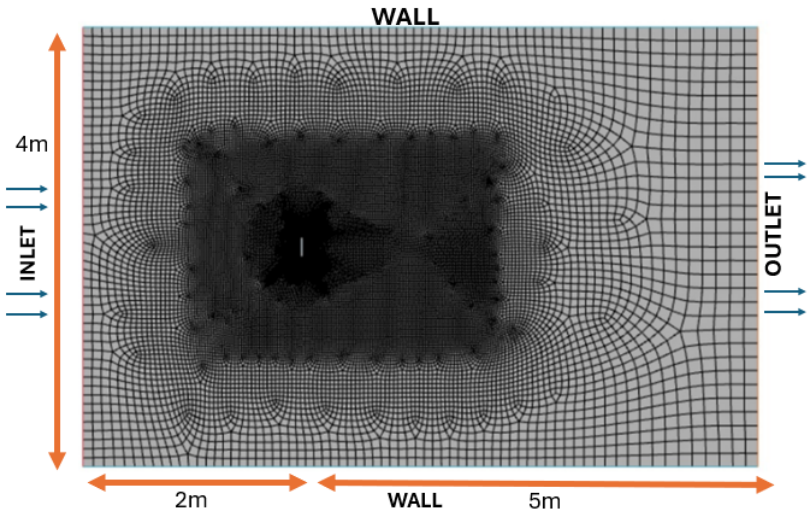

Figure 4.2: Example of an unstructured mesh and boundary conditions for steady flow simulations around a thin flat plate.

4.1.2. Oscillatory Flow Simulations

To represent wave-induced offshore conditions, oscillatory flow simulations were performed. The same flat plate was used, but now a time-dependent inlet velocity was prescribed to simulate sinusoidal oscillations [68]:

$$u(t) = U_{\max} \sin(\omega t). \tag{4.1}$$

A 2D domain extended about 5 m in all directions around the plate to capture oscillatory boundary layers and wake dynamics. Structured meshes were employed, often created by extruding a 3D structured mesh and then batching it into 2D to ensure uniform cell quality and refined near-wall resolution.

Key dimensionless parameters included the Keulegan-Carpenter (KC) number (ranging from 1 to 100) and Reynolds numbers on the order of 10^4. These were varied by adjusting $U_{\max}$, the period T, and the plate length L. Time steps were chosen adaptively based on the CFL condition, typically between 0.01 s and 0.001 s, for accurate resolution of each oscillation cycle.

$$KC = \frac{U_{\max} T}{L}, \tag{4.2}$$

$$Re = \frac{U_{\max} L}{\nu}, \tag{4.3}$$

Table 4.2: Boundary conditions for oscillatory flow simulations, implementing a sinusoidal velocity inlet.

Boundary	Condition
Inlet	$u(t) = U_{\max} \sin(\omega t)$
Outlet	Zero-gauge pressure outlet
Plate Surface	No-slip wall
Domain Walls	Symmetry

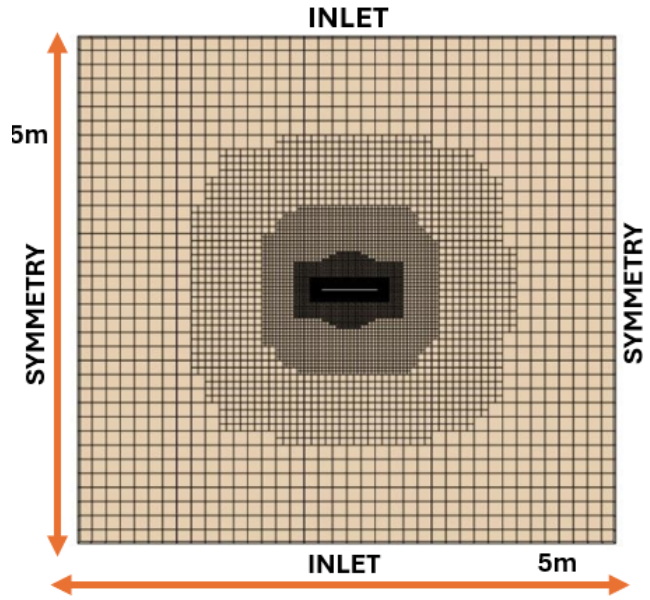

Figure 4.3: Example of an unstructured mesh and boundary conditions for oscillatory flow simulations.

Table 4.3: KC Number Dependency with Corresponding Periods, Angular Frequencies, and Amplitudes

KC Number	Period T (s)	ω (rad/s)	Amplitude A (m)
1.000	1.124	5.592	0.016
1.870	2.101	2.990	0.030
3.497	3.930	1.599	0.056
6.540	7.349	0.855	0.104
12.232	13.743	0.457	0.195
22.874	25.702	0.244	0.364
42.778	48.065	0.131	0.681
80.000	89.888	0.070	1.273

An unsteady implicit solver with adaptive time-stepping ensured stable convergence of residuals. The k-ω SST turbulence model provided improved accuracy for near-wall oscillatory flows [65]. Comparisons against literature-based benchmarks [68] confirmed that these simulations replicated key flow features such as vortex formation and shedding, validating the unsteady modeling approach.

4.1.3. Transition from 2D to 3D Full-Scale Simulations

Initial 2D simulations (steady and oscillatory) were essential for validating the CFD models and establishing baseline hydrodynamic coefficients. However, 2D simulations cannot fully capture the complex three-dimensional (3D) flow structures, vortex shedding, and turbulent wake interactions observed in real subsea environments. Additionally, relying solely on Reynolds number scaling to extrapolate 2D model-scale results to full-scale scenarios introduces uncertainties, as nonlinearities in fluid-structure interactions are not fully accounted for [66].

To address these limitations, the study progressed directly to full-scale CFD simulations. This transition began with 2D full-scale simulations, providing a controlled setting to assess hydrodynamic forces at operational scales. By first examining full-scale conditions in 2D, a baseline for drag forces and boundary layer development under realistic offshore conditions was established, informing subsequent

3D simulations.

Leveraging Stokes fifth-order wave theory [67], the 2D full-scale simulations ensured that Reynolds numbers and flow regimes matched realistic offshore conditions. Once confident with the 2D full-scale results, the methodology advanced to 3D full-scale simulations, overcoming the inherent limitations of 2D approximations. Computational domains were carefully defined to minimize boundary reflections while capturing wake vortex dynamics and flow separations around complex geometries. This comprehensive approach enabled a robust understanding of fluid-structure interactions governing dynamic installation performance under realistic marine conditions.

2D and 3D Full-Scale Mud Mat Simulations

Full-scale mud mat simulations, both 2D and 3D, were conducted under steady flow conditions to analyze drag forces acting normal to the incoming flow direction. The chosen inlet velocities (0.24–1.17 m/s) were derived using Stokes fifth-order wave theory, ensuring the replication of nonlinear wave profiles [67]. Computational domains were scaled appropriately to facilitate fully developed flow and wake formation while minimizing artificial boundary effects. For the 3D simulations, domain selection and refinement strategies were implemented to ensure that flow fields remained unaffected by boundary reflections.

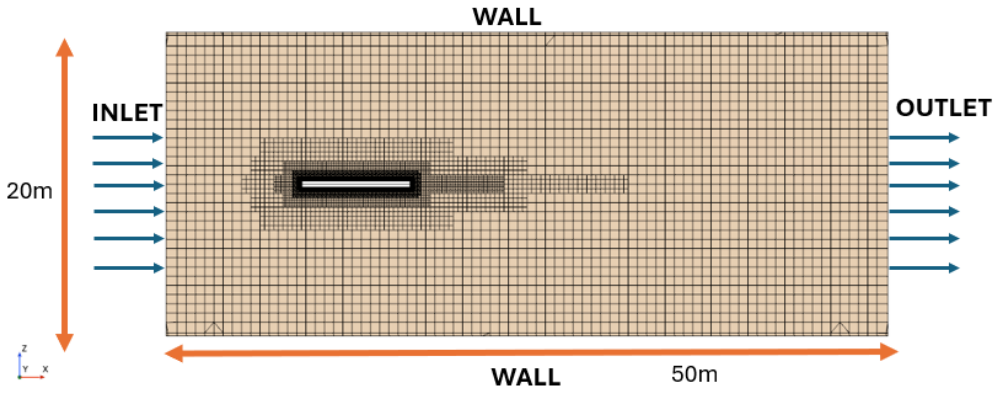

Figure 4.4: Full-scale 2D mesh for mud mat simulations.

Table 4.4: Summary of Flow and Structural Parameters

U_{max} (m/s)	KC	Period T (s)	Angular Frequency ω (rad/s)	H_s	H_{max} (m)	Amplitude (m)	KC_Amp	Reynolds Number ($\times 10^6$)
0.24	0.09	5	1.26	1.0	1.86	1.2566	0.5640	3.05
0.47	0.20	6	1.05	1.5	2.79	1.0472	0.4700	5.98
0.73	0.37	7	0.90	2.0	3.72	0.8976	0.4028	9.29
0.96	0.55	8	0.79	2.5	4.65	0.7854	0.3525	12.22
1.17	0.75	9	0.70	3.0	5.58	0.6981	0.3133	14.89

Table 4.5: Boundary conditions for mud mat simulations using velocities from Stokes fifth-order wave theory.

Boundary	Condition
Inlet	Velocity inlet (U_{inlet} from 0.24–1.17 m/s)
Outlet	Zero-gauge pressure outlet
Mud Mat Surface	No-slip wall
Top/Bottom (2D)	Wall boundaries
Sides (Left,Right)	Symmetry

For the 3D simulations, two aspect ratios (AR 0.8 and AR 2.0) and three orientations (0°, 90°, and inverted) were examined to evaluate geometric influences on hydrodynamic loading. Computational domains were designed to be sufficiently large to capture wake structures while minimizing reflections from domain boundaries. Refined meshing strategies—including surface remeshing, trimmed cell meshing, and prism layers—were applied near the mud mat surfaces to accurately capture boundary layer development and flow separations. Fluid properties were defined based on seawater conditions (density 1030 kg/m^3, dynamic viscosity 8.8871×10^{-4} Pa · s), and mesh independence tests confirmed that further refinement resulted in negligible changes to force predictions.

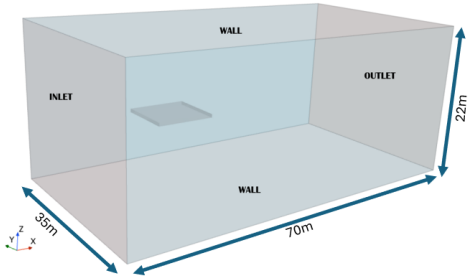

(a) Example domain configuration for AR 0.8

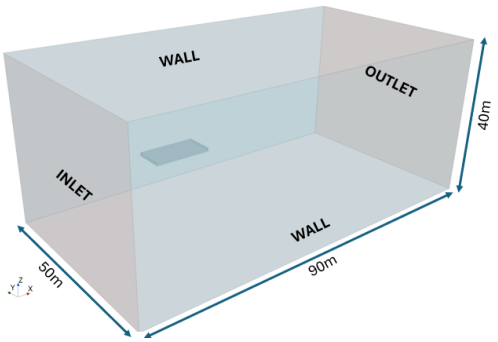

(b) Example domain configuration for AR 2.0

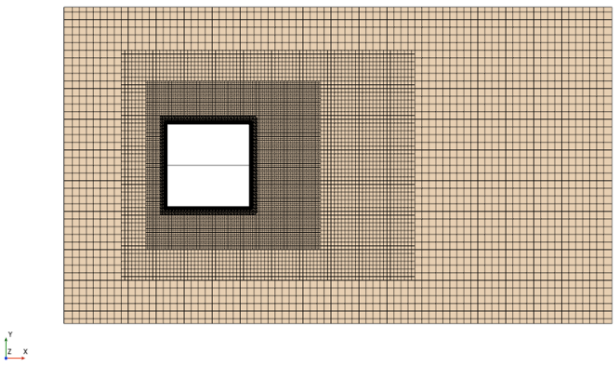

Figure 4.6: Refined mesh configuration for AR 0.8 mud mat simulations.

The k-ω SST turbulence model was used to ensure accurate predictions of flow separation and turbulence effects under steady flow conditions. In compliance with DNV guidelines [31], the primary focus remained on quantifying drag forces normal to the flow direction. Time series data of computed forces were recorded and analyzed using a least squares fitting approach to Morison's equation, allowing for the extraction of drag coefficients corresponding to each aspect ratio, orientation, and flow velocity. This structured methodology facilitated a detailed understanding of hydrodynamic performance, guiding

design considerations and improving the accuracy of structural assessments for offshore installation scenarios.

4.1.4. 3D Folded Mud Mat Simulations

The folded mud mat geometry (10 m × 3 m × 5 m) was analyzed using 3D steady-state CFD simulations to evaluate hydrodynamic forces during installation. The methodology followed a similar framework to that used for the full-scale mud mat simulations, with adjustments to account for the unique folded configuration and its transitional behavior during deployment.

The computational domain was defined to ensure sufficient space for wake development while minimizing boundary effects. The domain was discretized using trimmed cell meshing with prism layers near the mud mat surfaces to resolve boundary layers accurately. Volumetric refinements were introduced around the mud mat to capture localized flow features. Fluid properties were representative of seawater, with density 1030 kg/m^3 and dynamic viscosity 8.8871×10^{-4} Pa · s. Boundary conditions, derived from Stokes fifth-order wave theory, are summarized in Table 4.6.

Table 4.6: Boundary conditions for 3D folded mud mat simulations.

Boundary	Condition
Inlet	Velocity inlet (U_{inlet} from 0.24–1.17 m/s)
Outlet	Zero-gauge pressure outlet
Mud Mat Surface	No-slip wall
Top/Bottom (3D)	Wall boundaries
Sides (Left, Right)	Symmetry

The simulations employed a segregated steady-state RANS solver with the k-ω SST turbulence model to accurately predict near-wall flows and flow separation. Convergence was achieved when residuals fell below 10^{-6}, ensuring numerical stability and reliability. The time-averaged drag forces and hydrodynamic load distributions were extracted and analyzed to assess the performance of the folded configuration. The post-processing phase involved examining velocity and pressure fields to identify regions of high flow separation or adverse pressure gradients.

4.1.5. 3D Roller Guide Simulations

The 3D roller guide, measuring approximately 12 m in length and 1.2 m in height, was analyzed to evaluate hydrodynamic forces under steady flow conditions. This approach followed the same methodological frameworksubsection 4.1.3 used for previous full-scale simulations, with adjustments to accommodate the roller guide's asymmetric geometry and flow complexities near its edges.

The computational domain was defined to provide sufficient space for flow development and wake formation while minimizing boundary reflections. The geometry was discretized using trimmed cell meshing and prism layers near the guide surfaces to resolve boundary layers and capture localized flow features. Volumetric refinements were introduced around the roller guide to accurately represent regions of high shear and potential vortex formation.

Fluid properties were set to represent seawater, with density 1030 kg/m^3 and dynamic viscosity 8.8871×10^{-4} Pa · s. The inlet velocity was derived from Stokes fifth-order wave theory to ensure that the flow conditions were consistent with those applied in previous simulations. Boundary conditions are summarized in Table 4.7.

Table 4.7: Boundary conditions for 3D roller guide simulations.

Boundary	Condition
Inlet	Velocity inlet (U_{inlet} from 0.24–1.17 m/s)
Outlet	Zero-gauge pressure outlet
Roller Guide Surface	No-slip wall
Domain Walls	No-slip walls
Sides (Left, Right)	Symmetry

The k-ω SST turbulence model was used to resolve near-wall flow behavior and capture flow separation accurately. The solution was considered converged when residuals fell below 10^{-6}.

Velocity and pressure distributions were analyzed to identify shear regions and flow separation zones. The computed hydrodynamic forces were processed to extract drag coefficients, assessing the roller guide's response to installation conditions. These results aligned with previous findings, reinforcing the robustness of the applied methodology for subsea structure hydrodynamic evaluations.

4.2. Added Mass Simulations

Added mass represents the inertial contribution of an accelerated fluid surrounding a submerged structure. To quantify this effect, three-dimensional (3D) simulations were conducted for a flat plate representative of subsea mud mats. The computational domain extended from $(-25, -25, -20)$ m to $(25, 75, 20)$ m, ensuring minimal boundary reflection effects. A structured mesh with prism layers resolved boundary layers, while volumetric refinements captured flow details near the plate. Seawater properties were applied (density $1030\,\text{kg/m}^3$, viscosity $8.8871 \times 10^{-4}\,\text{Pa} \cdot \text{s}$). Boundary conditions are summarized in Table 4.8 adopted from [57].

Table 4.8: Boundary conditions for added mass simulations.

Boundary	Condition
Inlet (Bottom)	Time-dependent velocity (sinusoidal functions)
Outlet (Top)	Zero-gauge pressure
Plate Surface	No-slip wall
Side Walls	Symmetry

Sinusoidal inlet velocities ($u(t) = 0.24 \sin(1.26t)$ m/s) replicated oscillatory flow without mesh deformation, reducing computational cost. An implicit unsteady solver with adaptive time-stepping (CFL-conditioned) and the k-ω SST turbulence model resolved near-wall flows. Convergence criteria required residuals below 10^{-6}.

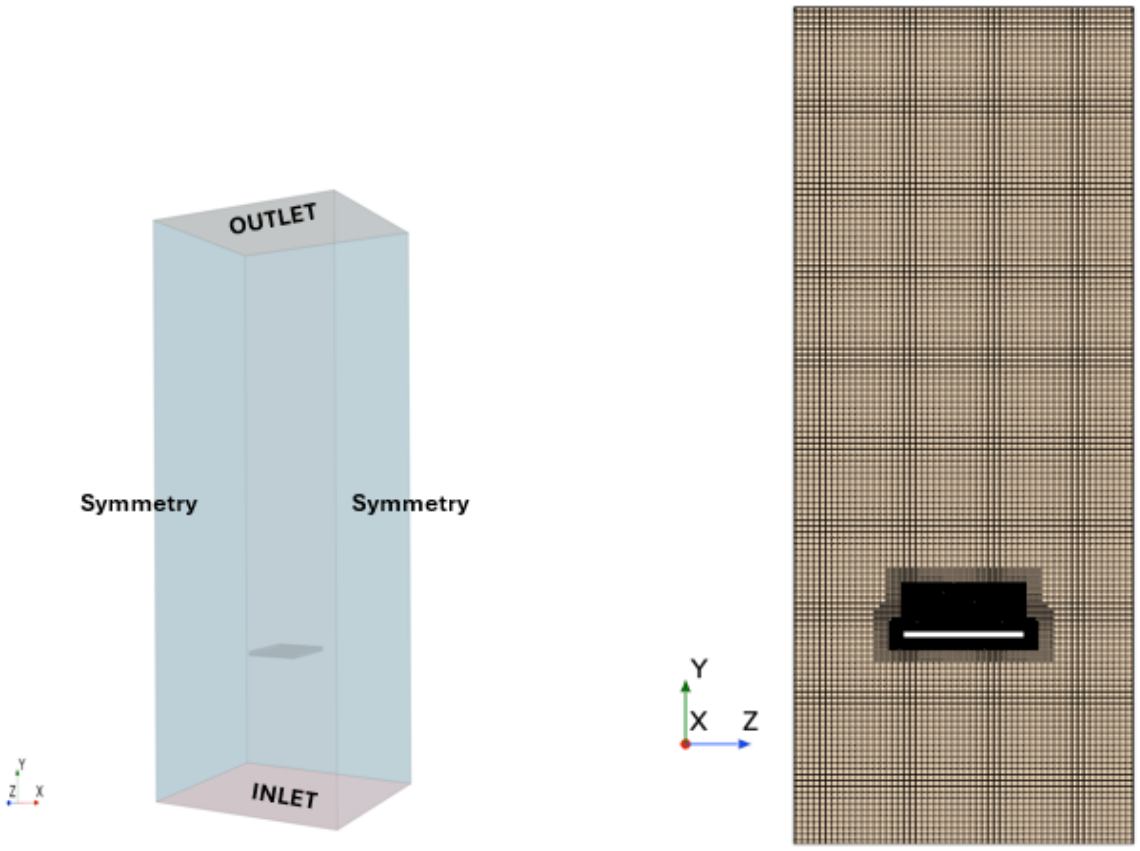

(a) Domain configuration.

(b) Mesh refinement near the plate.

Figure 4.7: Computational domain and mesh for added mass simulations.

Force data were extracted from time-averaged flow fields, with added mass coefficients (C_A) derived via least-squares fitting to Morison's equation. Table 4.9 details key simulation parameters. The methodology required 2000 iterations per case for convergence, demonstrating robustness for oscillatory flow analysis.

Table 4.9: Setup parameters for added mass simulations.

Parameter	Value	Description
Domain Size	$50\,\text{m} \times 100\,\text{m} \times 40\,\text{m}$	Extents
Mesh Cells	1.4M–1.6M	Trimmed cells with prism layers
Time Step	0.001–0.01 s	Adaptive CFL-based stepping
Inlet Function	$0.24\sin(1.26t)$	Primary oscillatory condition

Velocity/pressure field analysis validated the framework's capability to predict C_A, complementing steady-flow hydrodynamic coefficients. This consistency underscores CFD's utility for evaluating subsea structures across flow regimes.

4.3. Dynamic Installation Analysis of the J-Mode PLET

A dynamic installation analysis of the J-Mode Pipeline End Terminal (PLET) was conducted to assess structural behavior during installation under different sea states. Finite element analysis (FEA) was used to simulate the trajectory of the PLET from the splash zone to the seabed, incorporating

structural components such as the PLET, pipeline, vessel motions, and environmental conditions. Key factors influencing dynamic responses included wave-induced loads, added mass effects, and seabed interactions. A case study focusing on higher sea states, where excessive structural motions were induced, was analyzed to evaluate different hydrodynamic load prediction methods.

Detailed geometrical models of the full-scale PLET and pipeline were developed, maintaining consistency with the dimensions and properties used in full-scale CFD simulations. Hydrodynamic forces were calculated using both DNV guideline coefficients and CFD-derived coefficients. A comparative approach was employed to assess the influence of CFD-derived coefficients on predicted structural responses.

Wave conditions were modeled using Stokes fifth-order wave theory, ensuring accurate representation of nonlinear wave effects. Boundary conditions accounted for the transition from air to water at the free surface, incorporating slamming loads and added mass effects in the splash zone. The simulation accounted for six degrees of freedom, emphasizing vessel motions such as heave, pitch, and yaw, which significantly affect bending strains in the pipeline and structure. These motions were incorporated to simulate dynamic coupling between the vessel and the PLET during installation.

Two load cases were defined for comparative analysis: one using hydrodynamic coefficients from DNV guidelines and the other using CFD-derived coefficients. The impact of different hydrodynamic coefficients on structural response was assessed, particularly focusing on bending strains near the sagbend region. This analysis provided insights into the effect of improved hydrodynamic load predictions on installation workability and structural integrity. The results demonstrated that CFD-derived coefficients provided a refined representation of hydrodynamic forces, leading to noticeable differences in predicted structural responses. The case study underscored the necessity of integrating advanced hydrodynamic modeling techniques into dynamic installation analyses to enhance prediction accuracy and ensure safety during offshore installations.

5

Results & Discussion

This chapter presents the key findings from the CFD simulations and dynamic analyses conducted on subsea structures. It covers the results of steady and oscillatory flow simulations, the evaluation of hydrodynamic coefficients, and the implications of these findings on the design and installation of subsea structures.

5.1. Steady Flow Simulations

The 2D steady flow simulations aimed to validate the drag coefficient for a thin flat plate normal to the flow, comparing the results with values derived from DNV guidelines. At a flow velocity of 1 m/s, the calculated drag coefficient (C_D) was found to be 1.99, closely aligning with the expected DNV value of 1.9. This agreement underscores the reliability of the CFD model in accurately capturing hydrodynamic behavior under steady conditions.

The force-time history, shown in Figure 5.1, illustrates the stability of drag force measurements, confirming that steady-state conditions were achieved. The zoomed-in view further highlights the consistency of the forces over time, indicating minimal fluctuations once the flow reached equilibrium. This reinforces confidence in the accuracy and repeatability of the CFD approach for such configurations.

Post-processing of the simulation data included velocity contour plots (Figure 5.2), which revealed clear flow separation and wake formation behind the plate. These visualizations captured essential hydrodynamic phenomena, such as boundary layer separation and vortex formation, aligning well with physical expectations for such flows. The distinct wake region confirms that the CFD model effectively represents the interaction between the fluid and the plate, further validating the numerical approach.

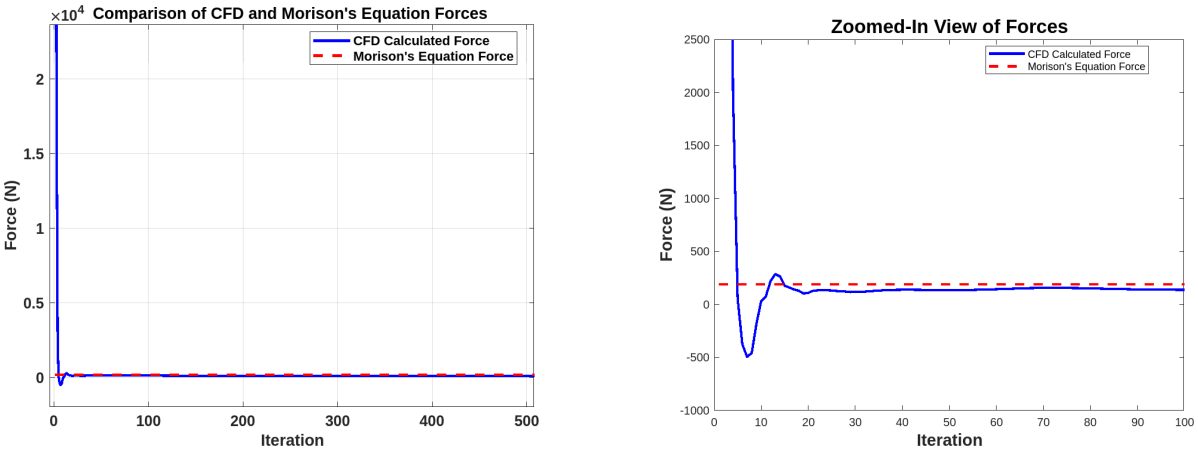

(a) Steady flow force time history.

(b) Zoomed-in view for first 100 iterations.

Figure 5.1: Force time history for steady flow normal to the plate at 1 m/s.

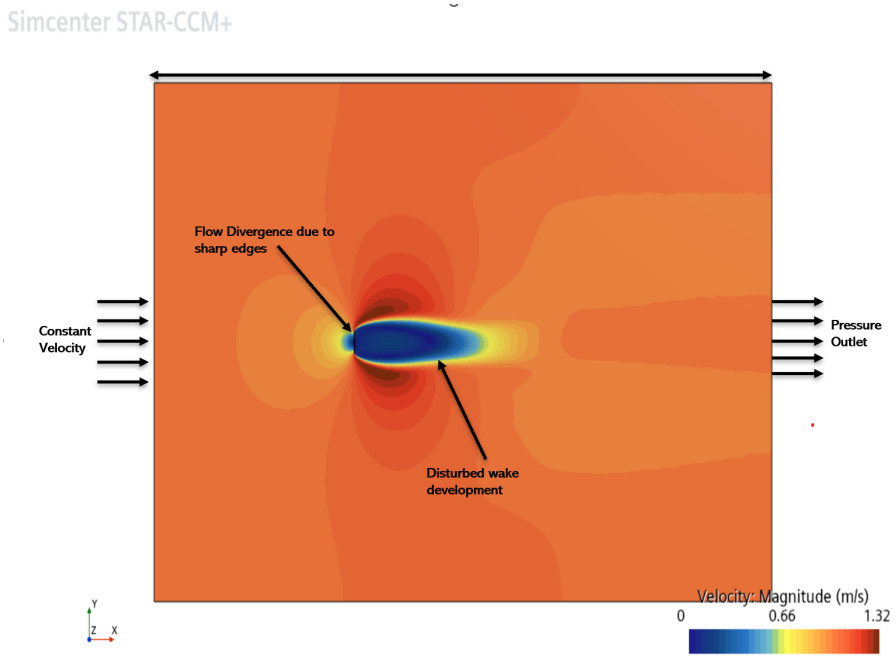

Figure 5.2: Velocity contour plot showing flow separation and wake formation behind the flat plate at 1 m/s.

These results demonstrate that the steady flow simulations provide an accurate basis for validating drag coefficients, reinforcing the suitability of the CFD model for predicting hydrodynamic forces. This foundational analysis serves as a precursor to more complex studies, such as oscillatory flow simulations, where dynamic effects become significant.

5.2. Oscillatory Flow Simulations

Oscillatory flow simulations were conducted to evaluate the hydrodynamic coefficients over a range of Keulegan-Carpenter (KC) numbers from 1 to 80, as described in subsection 4.1.2. The simulations aimed to determine the drag (C_D) and inertia (C_M) coefficients for the flat plate under oscillatory flow conditions, which are critical for predicting forces on structures subjected to wave-induced motions.

The hydrodynamic force on the plate was extracted from the simulations and fitted to the Morison equation:

$$F(t) = \frac{1}{2}\rho C_D A U(t)|U(t)| + \rho C_M V \frac{dU(t)}{dt}, \tag{5.1}$$

where $F(t)$ is the total force, $U(t)$ is the instantaneous velocity, A is the reference area, V is the displaced volume, and $\frac{dU(t)}{dt}$ is the acceleration.

The values of C_D and C_M were determined for each KC number by fitting the CFD-calculated forces to the Morison equation using a least-squares method. Table 5.1 summarizes the results.

Table 5.1: Drag and inertia coefficients obtained from oscillatory flow simulations for various KC numbers.

KC Number	Drag Coefficient (C_D)	Inertia Coefficient (C_M)
1.00	12.4	2.1
1.87	10.2	2.39
3.49	9.0	2.59
6.54	8.03	2.11
12.23	4.11	1.62
22.87	3.88	2.36
42.77	3.66	2.89
80.00	3.41	3.86

Figures 5.3 and 5.4 present the velocity contour plot and the comparison between CFD-calculated forces and the fitted Morison forces for selected KC numbers.

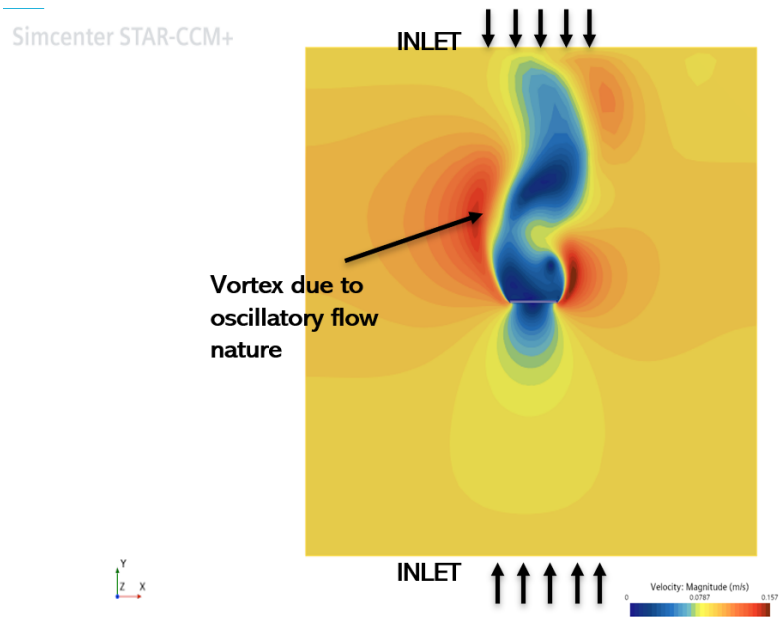

Figure 5.3: Velocity contour plot during oscillatory flow at KC = 12.23,

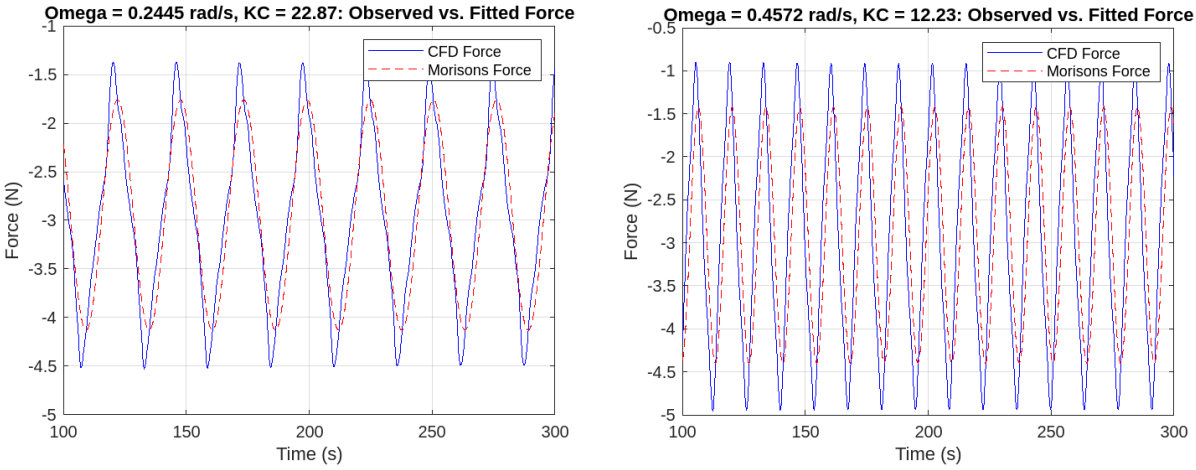

(a) KC = 22.87, $\omega = 0.2445\,\mathrm{rad/s}$ **(b)** KC = 12.23, $\omega = 0.4572\,\mathrm{rad/s}$

Figure 5.4: Comparison of CFD-calculated hydrodynamic forces and fitted Morison equation forces for different KC numbers.

The variation of drag and inertia coefficients with KC number is presented in Figure 5.5. The results show that the drag coefficient decreases with increasing KC number, while the inertia coefficient exhibits a more complex relationship, reflecting the transition between drag-dominated and inertia-dominated flow regimes.

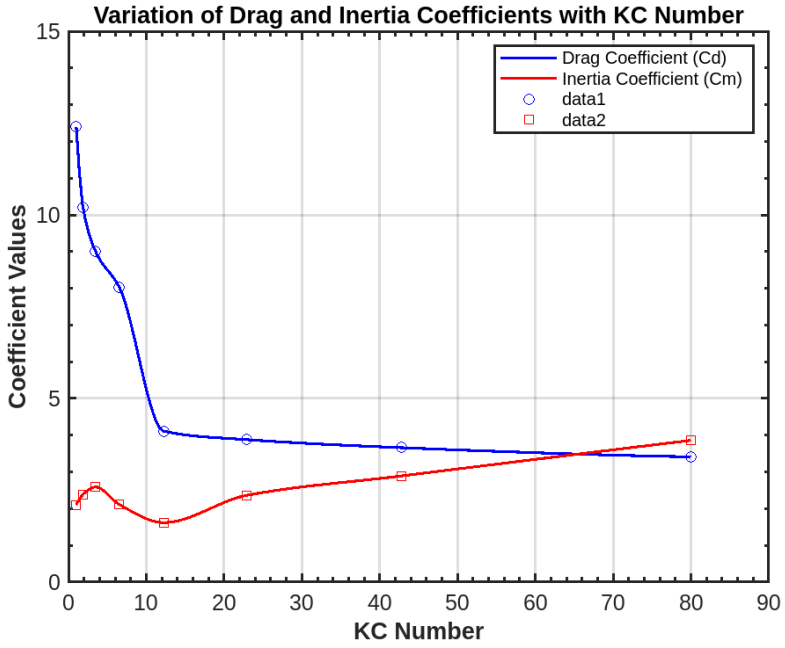

Figure 5.5: Variation of drag (C_D) and inertia (C_M) coefficients with KC number

To facilitate comparison with established empirical data, the CFD results were compared with reference data from [47, 45]. Figures 5.6a and 5.6b display this comparison.

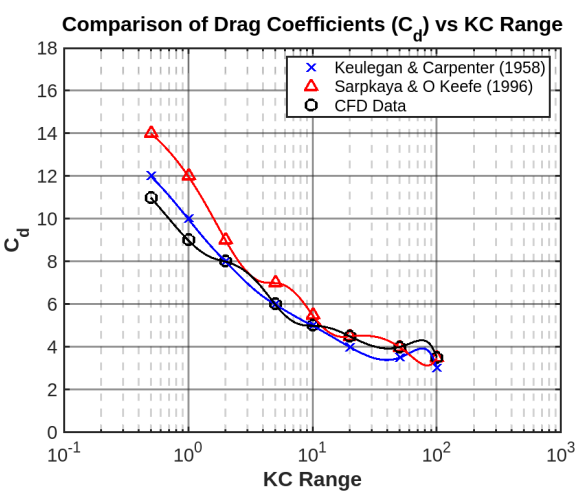

(a) Drag coefficient (C_D) vs. KC number

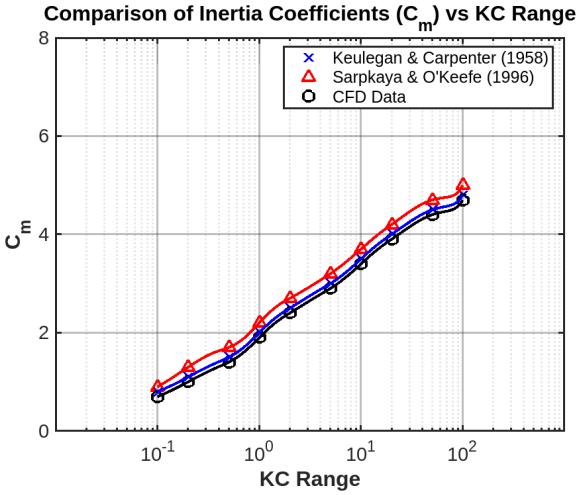

(b) Inertia coefficient (C_M) vs. KC number

Figure 5.6: Comparison of CFD-derived hydrodynamic coefficients with experimental data.

The CFD results closely matched the trends observed in experimental studies, validating the CFD approach for predicting hydrodynamic coefficients under oscillatory flow conditions.

5.3. Full-Scale Simulations

The full-scale simulations of subsea structures, including mud mats, roller guides, and folded mud mats, were conducted under realistic sea states using flow conditions and wave kinematics derived from Stokes' fifth-order wave theory. These conditions mirror those considered in the dynamic J-mode PLET installation simulations, providing a consistent basis for evaluating hydrodynamic performance. By modeling simplified components like mud mats, which approximate the PLET's dimensions, a detailed assessment of hydrodynamic loads was achieved, supporting the accurate prediction of forces and moments critical to subsea installations.

Table 5.2: Flow Conditions for Full-Scale 3D Folded Mud Mat Simulations

Umax (m/s)	KC	T (s)	omega (rad/s)	Hs (m)	Hmax (m)	Amplitude	KC_AMP	Re No ($\times 10^6$)
0.24	0.09	5	1.26	1	1.86	1.26	0.564	3.05
0.47	0.20	6	1.05	1.5	2.79	1.05	0.470	5.98
0.73	0.37	7	0.90	2	3.72	0.90	0.403	9.29
0.96	0.55	8	0.79	2.5	4.65	0.79	0.352	12.22
1.17	0.75	9	0.70	3	5.58	0.70	0.313	14.89

5.3.1. 2D vs 3D Mud Mat Simulations

The transition from 2D to 3D full-scale simulations was essential to capture the complete hydrodynamic behavior under realistic flow conditions. While 2D simulations provided initial insights into drag forces and coefficients, they did not account for the full complexity of fluid-structure interactions. The 3D simulations, shown in Figure 5.7, consistently exhibited higher drag forces due to the inclusion of spanwise vortex shedding and additional flow separation zones. The increasing discrepancy at higher velocities highlights the importance of 3D effects in realistic subsea conditions. These findings demonstrate that relying on 2D simulations may lead to non-conservative designs, particularly at higher velocities where 3D effects become more pronounced. Thus, 3D simulations are necessary for accurate hydrodynamic performance predictions.

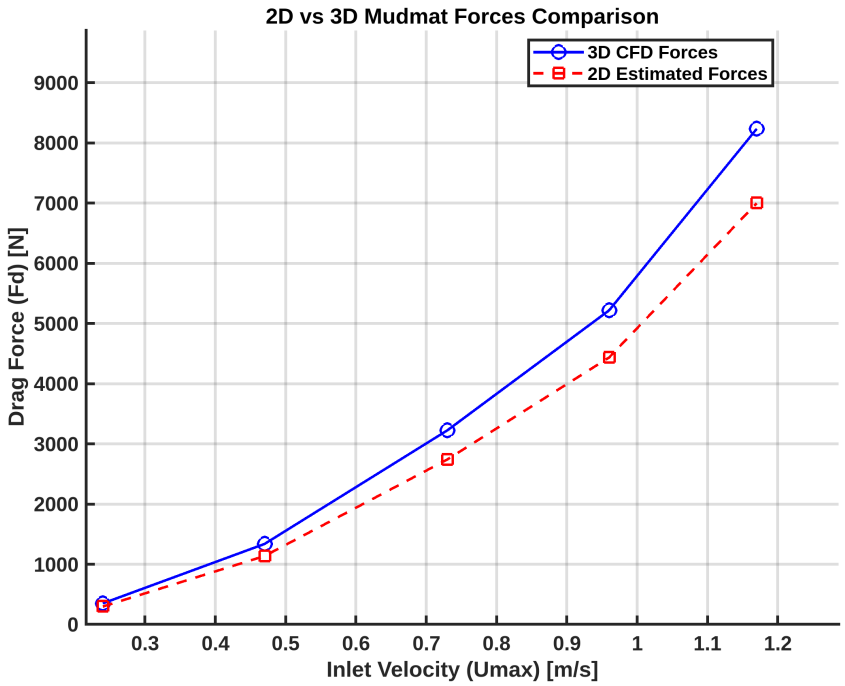

Figure 5.7: Comparison of drag forces between 2D and 3D full-scale mud mat simulations.

5.3.2. 3D Full-Scale Mud Mat Simulations at 0° Orientation

Simulations for aspect ratios (AR) of 0.8 and 2.0 were performed at 0° orientation to assess the hydrodynamic forces under various flow conditions. The comparison of drag forces, presented in Figure 5.8, shows a quadratic relationship between drag force and velocity, with AR 0.8 consistently experiencing higher drag due to increased flow resistance. This emphasizes the impact of aspect ratio on drag characteristics, where lower aspect ratios exhibit more flow separation and turbulence.

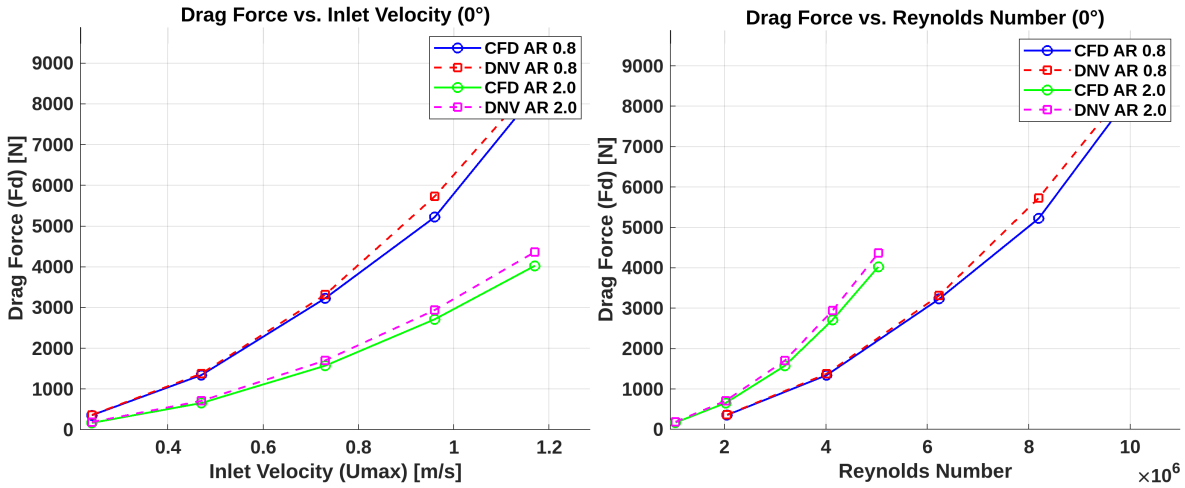

Figure 5.8: (Left) Drag Force vs. Inlet Velocity for AR 0.8 and 2.0 at 0° orientation. (Right) Drag Force vs. Reynolds Number for AR 0.8 and 2.0 at 0° orientation.

Analysis of Drag Forces: The drag forces follow theoretical expectations, with higher forces observed for AR 0.8 due to more pronounced flow disturbances. The deviation from DNV predictions at higher Reynolds numbers (Figure 5.8, right) highlights the limitations of empirical models, particularly in

complex geometries.

Drag Coefficient Analysis: The drag coefficients, shown in Figure 5.9, exhibit a stable trend across velocities, though CFD values are slightly lower than DNV's. The underprediction by CFD for AR 0.8 suggests that further refinement in turbulence modeling may be required. The goodness of fit for AR 2.0 decreases as aspect ratio increases, indicating that higher complexity in flow structures requires more detailed modeling.

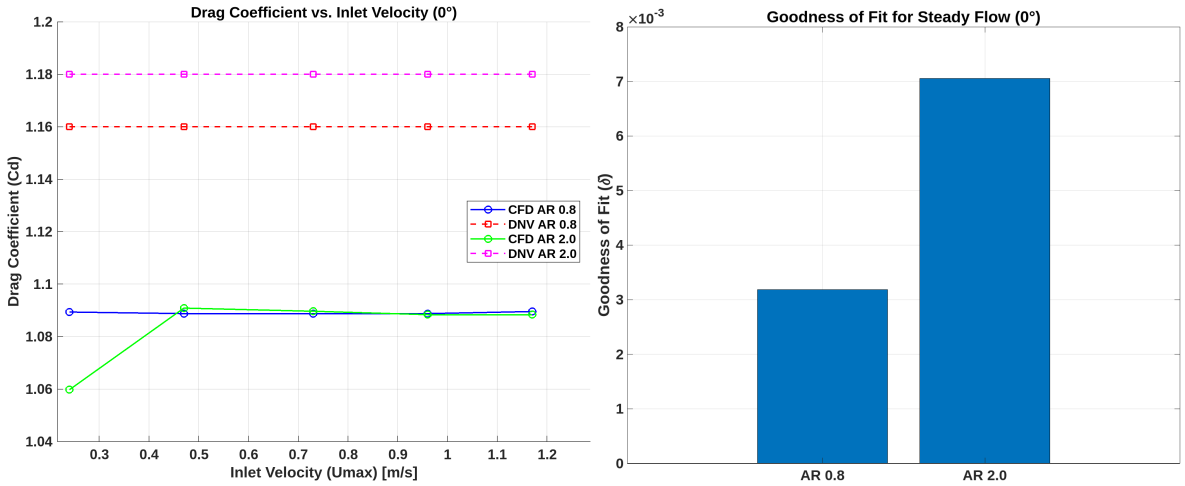

Figure 5.9: (Left) Drag Coefficient vs. Inlet Velocity for AR 0.8 and 2.0 at 0° orientation. (Right) Goodness of Fit for Steady Flow at 0° orientation.

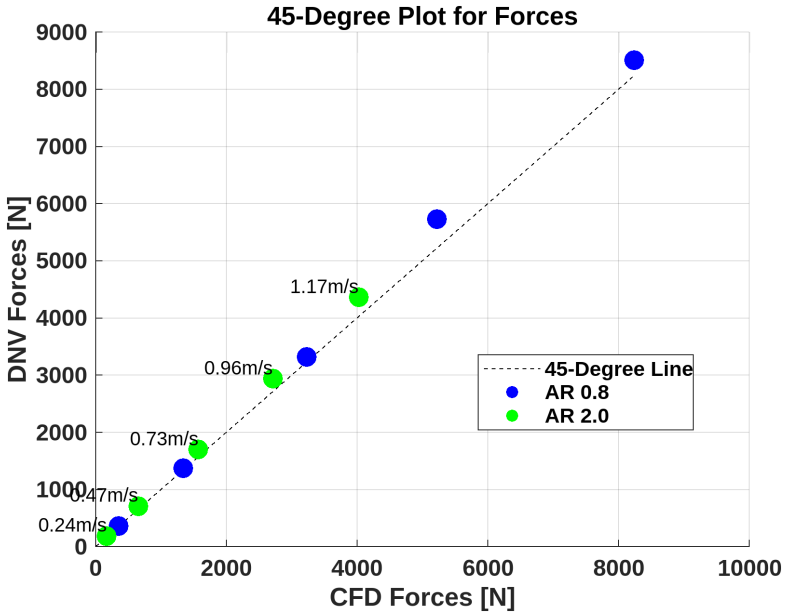

Figure 5.10: Comparison of CFD and DNV Forces across AR 0.8 and AR 2.0 at various velocities plotted against a 45-degree line indicating ideal agreement.

Figure 5.10 highlights the deviations between CFD-derived forces and DNV predictions, particularly for AR 0.8 at higher velocities. The results show that relying solely on empirical coefficients may oversimplify flow dynamics, stressing the importance of CFD simulations in providing a more accurate prediction for non-standard configurations.

5.3.3. 90 Degree Orientation of Full-Scale Mud Mat Simulations

The 90-degree orientation simulations emphasize the effect of perpendicular flow conditions on the hydrodynamic behavior of mud mats with aspect ratios (AR) of 0.8 and 2.0. In this orientation, the broad side of the mud mat is fully exposed to the flow, resulting in higher drag forces due to the larger surface area facing the fluid. Figures 5.11 illustrates the drag forces experienced by the mud mats across a range of Reynolds numbers and inlet velocities. The CFD results exhibit a clear trend of increasing drag force with rising Reynolds numbers and velocities, consistent with theoretical expectations. Notably, CFD-derived drag forces, for both k-ω and k-ϵ turbulence models, exceed the DNV predictions, reflecting the additional complexity in real-world fluid interactions that DNV coefficients may simplify.

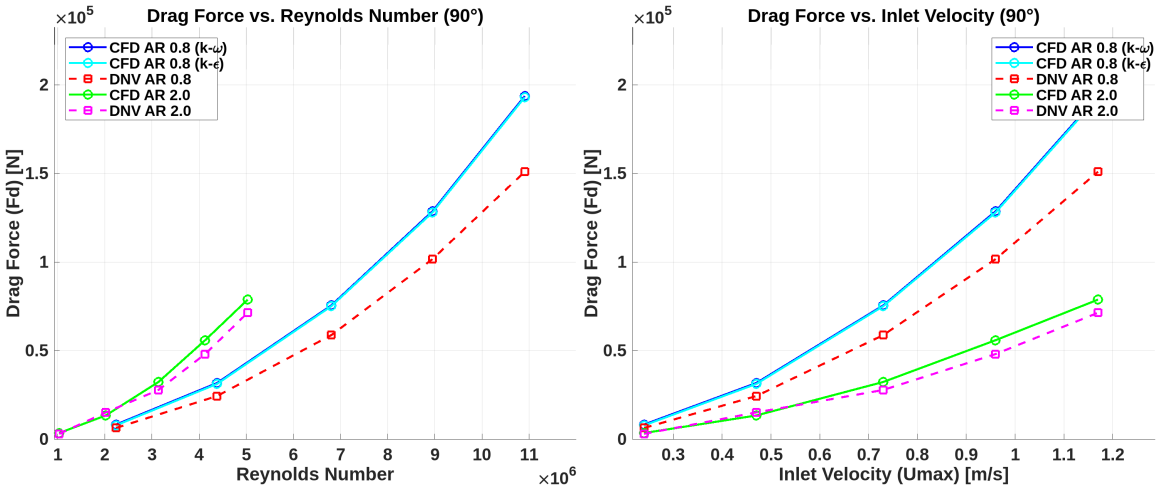

Figure 5.11: Drag Force vs. Reynolds Number and Inlet Velocity at 90° Orientation for AR 0.8 and 2.0.

Comparison of Drag Coefficients

Figure 5.12 presents the drag coefficients (C_D) against inlet velocity. The results show that the drag coefficients from CFD simulations using the k-ω model are higher than those from the k-ϵ model and the DNV values, especially for AR 0.8. This indicates that the k-ω model better captures the flow separation and reattachment dynamics, which are critical at higher angles of attack and complex flow conditions.

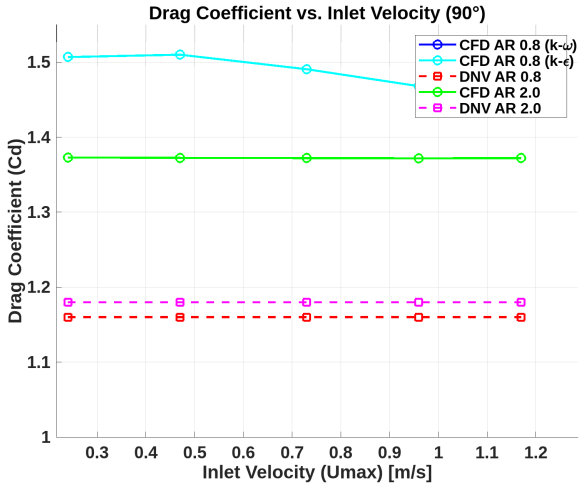

Figure 5.12: Drag Coefficient (C_D) vs. Inlet Velocity at 90° Orientation.

45-Degree Comparison and Goodness of Fit

The 45-degree plot (Figure 5.13) compares CFD and DNV forces, showing that CFD consistently predicts higher forces than DNV standards across all velocities, reflecting the conservative nature of DNV guidelines. The Goodness of Fit plot further demonstrates the accuracy of CFD models, with AR 0.8 showing a closer fit with the k-ω model than the k-ϵ model.

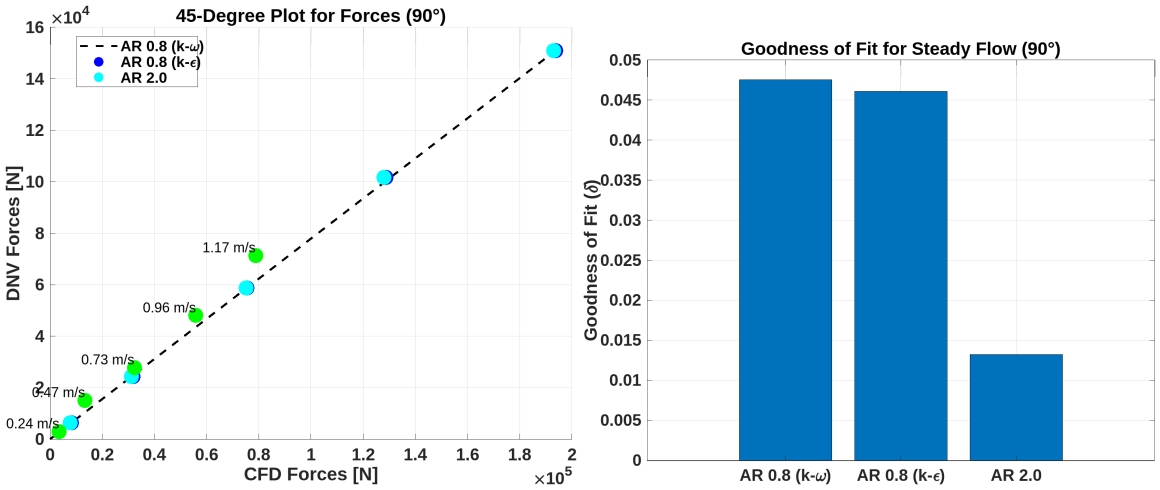

Figure 5.13: 45-Degree Plot of Forces and Goodness of Fit for Steady Flow at 90° Orientation.

The higher drag forces predicted by the k-ω model underline its effectiveness in capturing the intricate flow separation and reattachment dynamics around bluff bodies in perpendicular orientations. The significant discrepancies between CFD and DNV forces suggest that relying solely on empirical DNV coefficients may underestimate drag forces. Therefore, detailed CFD modeling becomes crucial for a more realistic evaluation of hydrodynamic loads, particularly in critical subsea installation scenarios. The results emphasize that empirical coefficients might oversimplify real-world fluid interactions, and CFD offers a more robust and accurate prediction in such complex orientations.

5.3.4. Breadth-Inverted Orientation

The simulations for the breadth-inverted orientation were performed to evaluate the hydrodynamic behavior of mud mats at different aspect ratios (AR) of 0.8 and 2.0. These tests primarily focused on variations in drag forces and coefficients across different Reynolds numbers and inlet velocities. Figures 5.14 and 5.14 provide a comparative analysis of drag forces between CFD-derived and DNV-derived values for both aspect ratios.

For AR 0.8, the CFD simulations, using both the k-ϵ and k-ω turbulence models, showed a close agreement with the DNV trends. However, CFD values displayed a slight under-prediction of forces at higher velocities, which can be attributed to more refined near-wall treatment employed in the CFD models, especially for turbulence effects at higher Reynolds numbers. Conversely, for AR 2.0, the CFD results closely aligned with DNV predictions, indicating a lesser sensitivity to the aspect ratio change compared to the 0-degree and 90-degree orientations.

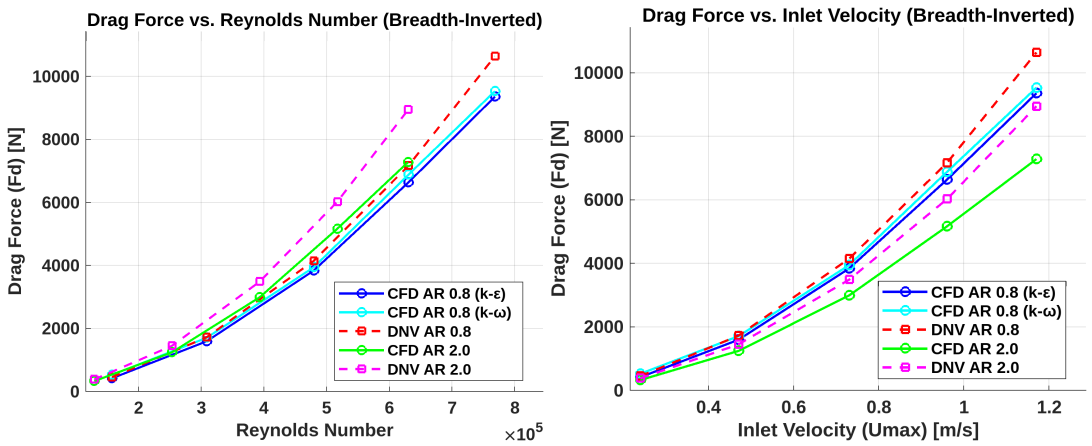

Figure 5.14: Comparison of drag forces vs. Reynolds number (left) and inlet velocity (right) for the breadth-inverted orientation.

As depicted in Figure 5.14, for AR 0.8, the drag forces predicted by CFD align well with DNV values at lower velocities but diverge slightly as velocity increases, which suggests that the CFD model better captures the flow separation and wake dynamics at higher Reynolds numbers. In contrast, for AR 2.0, both CFD and DNV results are in close agreement, highlighting that larger aspect ratios may reduce the influence of complex flow separations, leading to more streamlined flow patterns around the structure.

Figure 5.15 illustrates the variation in drag coefficients with inlet velocity. For AR 0.8, CFD simulations predicted consistently lower drag coefficients than the DNV values, likely due to the finer resolution of flow characteristics in the CFD models, particularly in capturing the wake effects and separation zones. For AR 2.0, the drag coefficients remained lower as the increased aspect ratio contributed to more stable flow around the structure, reducing the overall hydrodynamic resistance.

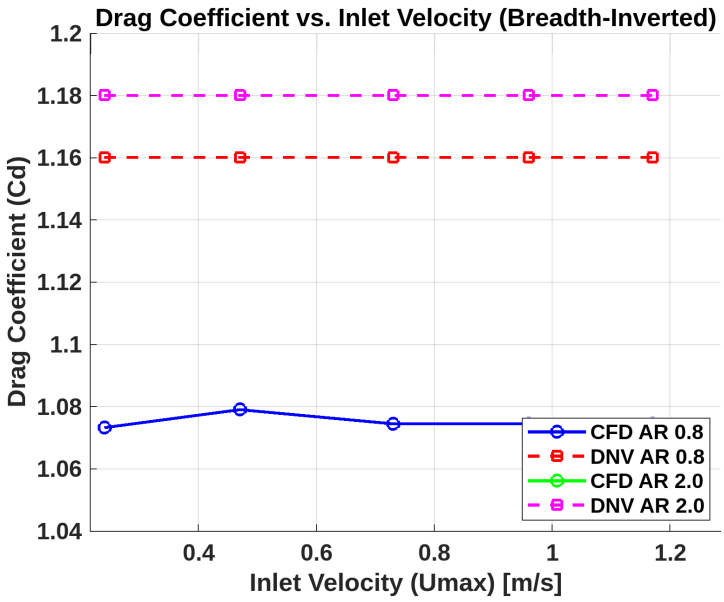

Figure 5.15: Drag Coefficient (C_D) vs. Inlet Velocity for the breadth-inverted orientation.

The goodness of fit analysis for steady flow simulations is shown in Figure 5.16. The results for AR 0.8 using the k-ϵ model exhibit the least deviation, confirming the accuracy of this turbulence model in capturing the flow physics more effectively, particularly in moderate flow conditions. Figure 5.16

compares CFD and DNV forces across velocities, demonstrating a strong agreement between the two methods for both aspect ratios. This alignment highlights the reliability of the CFD model in approximating forces for breadth-inverted configurations, further validating the applicability of CFD in subsea structure analysis.

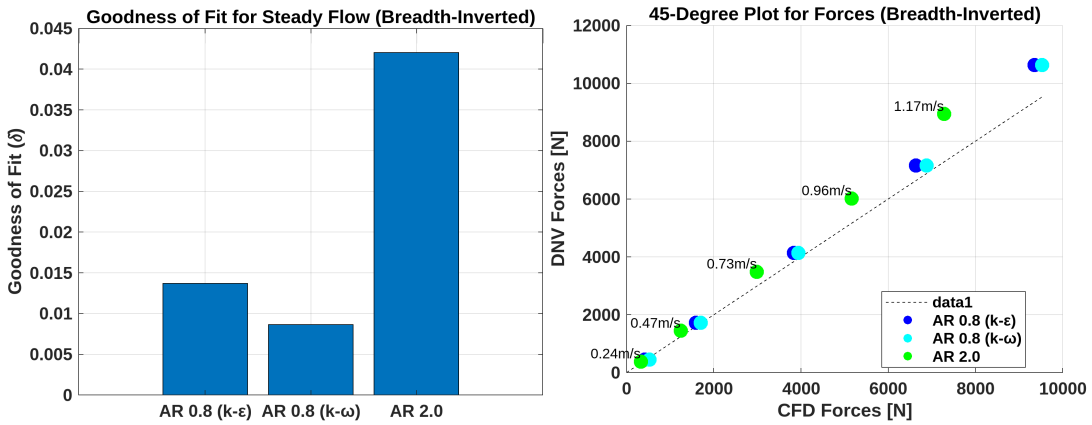

Figure 5.16: Goodness of fit for steady flow (left) and 45-degree plot of forces (right) for the breadth-inverted orientation.

From the results, it is evident that the breadth-inverted orientation presents distinct hydrodynamic characteristics compared to the 0-degree and 90-degree orientations. Both drag force predictions and drag coefficient analyses align well between CFD and DNV for the two aspect ratios. However, the lower drag coefficients predicted by CFD highlight the ability of the model to capture finer flow details around the structure, especially for AR 0.8. The findings demonstrate that increasing the aspect ratio (AR 2.0) consistently reduces the hydrodynamic forces, suggesting that this configuration could serve as a potential design optimization strategy for subsea structures in breadth-inverted orientations. Also, the selection of the turbulence model (k-ϵ vs. k-ω) proves critical, as it significantly influences the accuracy of the force predictions, particularly under adopted varying flow conditions.

5.3.5. Folded Mudmat and Roller Guides

The full-scale simulations of the folded mudmat and roller guides provide critical insights into the hydrodynamic behavior of these subsea structures under varying flow conditions. By comparing CFD-derived results with those obtained using DNV empirical models, the limitations and applicability of traditional methods in complex flow scenarios become evident, particularly for non-standard geometries such as these.

For the folded mudmat, the CFD simulations showed a close alignment with DNV predictions across the tested range of inlet velocities and Reynolds numbers. Figures 5.17a and 5.17b illustrate the linear dependence of drag force on both velocity and Reynolds number. The minor deviations observed can be attributed to potential boundary layer effects or flow separation phenomena, which are not fully captured by DNV's simplified empirical estimations.

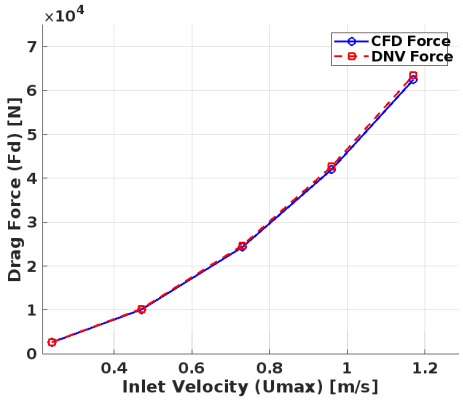

(a) Drag Force vs. Inlet Velocity

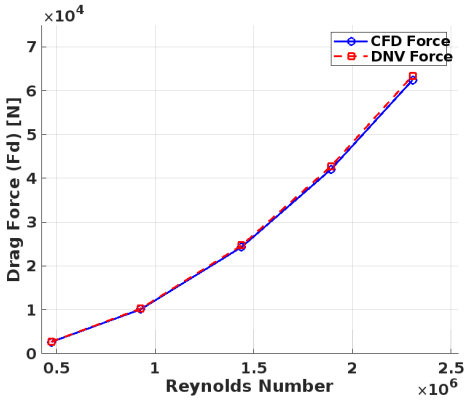

(b) Drag Force vs. Reynolds Number

Figure 5.17: Folded Mudmat: Drag force comparison between CFD and DNV predictions.

The drag coefficient plots (Figure5.18a) reveal a consistent underestimation by CFD compared to DNV values, which suggests that the CFD model captures more refined flow dynamics, particularly in regions of flow separation and turbulence, leading to a lower overall drag profile. This underprediction, while minor, indicates that CFD offers a more precise assessment of the hydrodynamic behavior, especially for complex subsea structures like folded mudmats, where three-dimensional flow phenomena are significant.

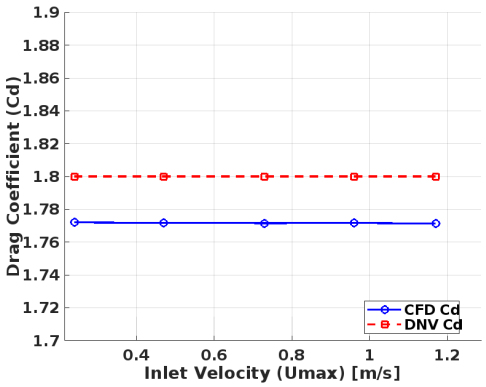

(a) Drag Coefficient vs. Inlet Velocity

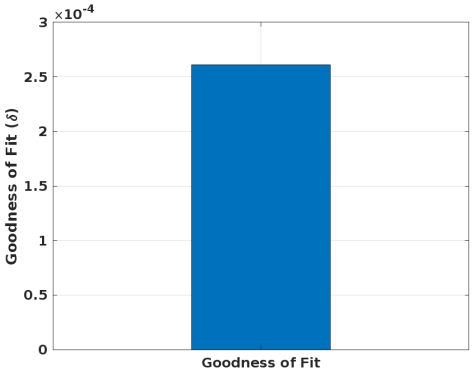

(b) Goodness of Fit for Folded Mudmat

Figure 5.18: Folded Mudmat: Drag coefficients and goodness of fit analysis.

The hydrodynamic performance of the roller guides presented more significant discrepancies between CFD and DNV forces, particularly at higher velocities. As shown in Figures 5.19a and 5.19b, the CFD simulations consistently predicted lower drag forces than those estimated by DNV. This discrepancy is likely due to the complex flow interactions, including turbulence and vortex shedding, around the roller guides, which are not adequately captured by the DNV empirical models.

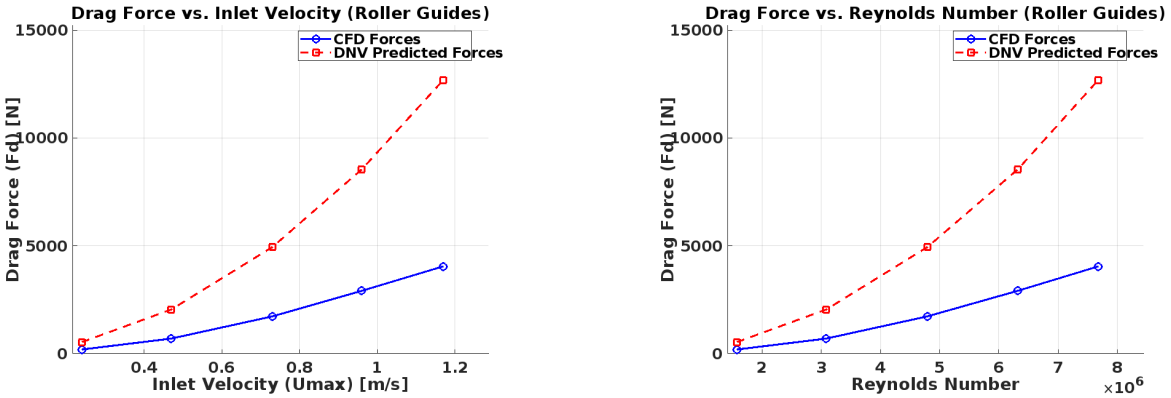

(a) Drag Force vs. Inlet Velocity

(b) Drag Force vs. Reynolds Number

Figure 5.19: Roller Guides: Drag force comparison between CFD and DNV predictions.

As indicated in Figure 5.20, the drag coefficients obtained from CFD were significantly lower than those from DNV estimations, suggesting that the DNV empirical coefficients may overestimate the forces acting on roller guides. This could lead to overly conservative designs that do not fully leverage the true hydrodynamic performance of the guides. The refined resolution of flow phenomena in the CFD models, particularly in capturing the intricate wake dynamics and turbulence, likely contributes to the lower drag coefficients predicted by CFD.

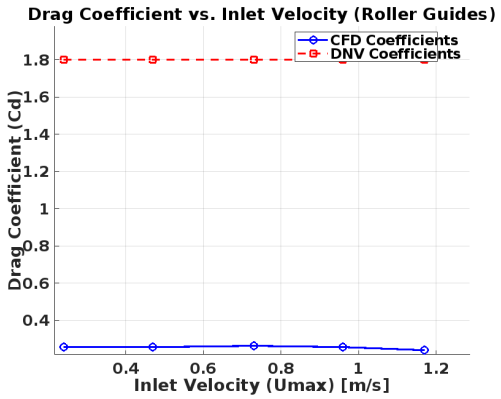

Figure 5.20: Drag Coefficient vs. Inlet Velocity for Roller Guides.

Overall, the full-scale simulations of both the folded mudmat and roller guides underscore the value of CFD in providing a more nuanced understanding of the fluid-structure interactions in subsea environments. While the folded mudmat simulations demonstrate close agreement with DNV predictions, the roller guides show significant deviations, particularly at higher velocities, highlighting where traditional empirical models may fall short. The CFD simulations offer a more precise assessment of the hydrodynamic forces, especially in capturing the complex flow dynamics that influence drag coefficients and overall performance. These findings suggest that reliance on empirical models alone may result in non-optimal designs for subsea installations, advocating for the integration of advanced CFD techniques in the design and analysis of such structures.

5.4. Added Mass Results

The added mass simulations were performed for three different sea states, each characterized by varying Keulegan-Carpenter (KC) numbers and oscillatory flow conditions. The KC numbers ranged from 0.9 to 0.75, with corresponding frequencies of 1.26 rad/s, 0.90 rad/s, and 0.70 rad/s. The amplitudes for the oscillatory flow used in these simulations were 0.24 m, 0.73 m, and 1.15 m, respectively. The added mass coefficient (C_a) and drag coefficient (C_d) were obtained by applying a least-squares fitting approach to Morison's equation, providing insight into the hydrodynamic loads acting on the structure.

Table 5.3: Fitted Coefficients for Added Mass Simulations.

Sea-State	KC Number	Drag Coefficient (C_d)	Added Mass Coefficient (C_a)
1	0.9	45.2	22.5
2	0.37	78.9	9.4
3	0.75	204.5	0.8

The fitted drag coefficient (C_d) generally increases as the KC number decreases, indicating the heightened influence of inertia as the oscillatory motion becomes more dominant. This trend is consistent with the physics of added mass, where larger amplitudes and lower frequencies amplify inertial forces acting on the structure. In contrast, the added mass coefficient (C_a) demonstrates varying and, in some cases, negative values. The negative C_a values suggest potential phase differences between the fluid forces and the structure's motion, which may result from complex flow phenomena such as flow separation and vortex shedding that are not fully captured by the simplified linear assumptions of Morison's equation.

Figure 5.21 illustrates the differences between the forces predicted by CFD simulations and those obtained through fitting Morison's equation for each sea state. While the fitting approach successfully captures the overall trend of force oscillations, there are noticeable discrepancies in amplitude, particularly for higher KC numbers. These discrepancies arise due to the limitations of Morison's equation in accounting for complex interactions such as flow separation, vortex dynamics, and fluid-structure coupling that are prominent under oscillatory flow conditions. The phase mismatches observed in the force-time histories further underscore the importance of incorporating more advanced fluid-structure interaction models, as linear approximations like Morison's equation fail to fully capture the non-linear behavior of the fluid forces acting on the structure.

Unlike steady flow simulations where drag dominates, oscillatory flow introduces significant added mass effects due to the continuous acceleration and deceleration of the surrounding fluid. In this context, added mass becomes a critical factor in determining the total hydrodynamic load. The fitted coefficients, as seen in Table 5.3, reflect the challenge of accurately predicting the dynamic interactions between the structure and the oscillating fluid. The fact that C_a shows wide variability, including negative values, highlights the complex physics at play. These values suggest that the inertia-induced forces are not always in phase with the structural motion, leading to fluctuations in the effective added mass. This is a critical finding, as it shows the limitations of simplified empirical models like Morison's equation when applied to dynamic installation scenarios in offshore environments.

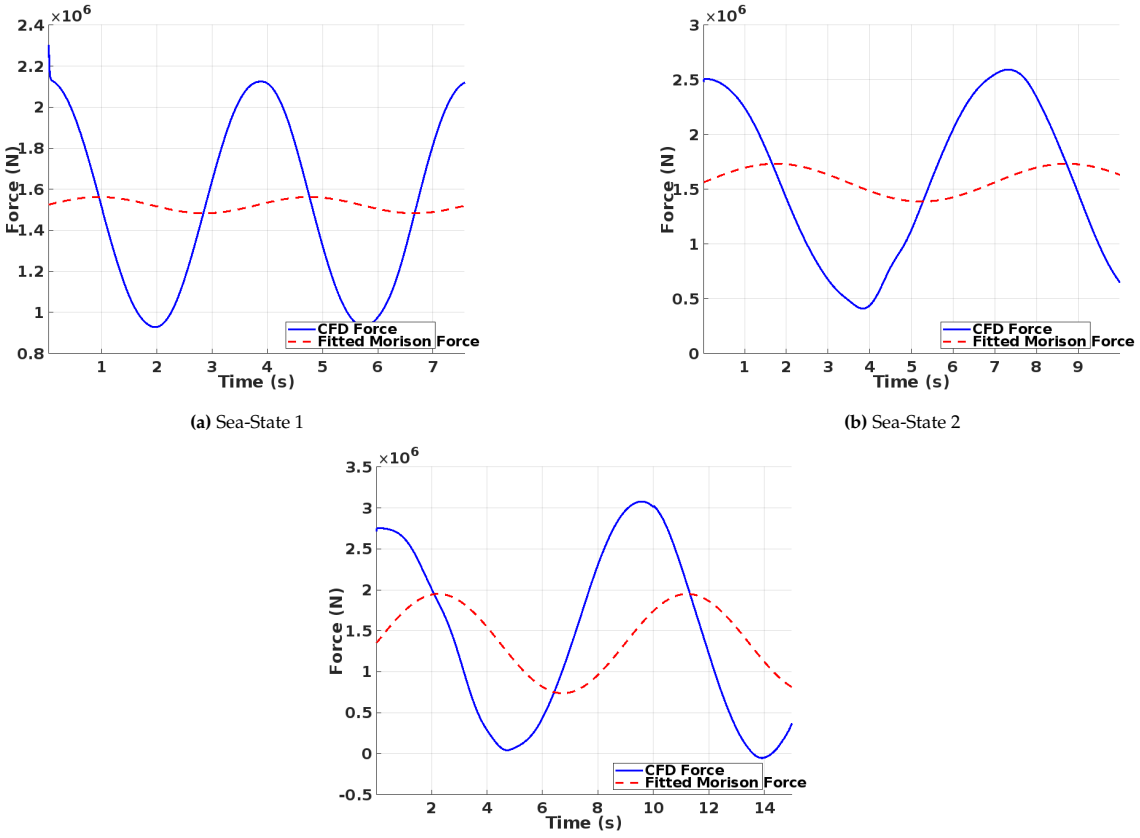

(a) Sea-State 1

(b) Sea-State 2

(c) Sea-State 3

Figure 5.21: Comparison of CFD and Fitted Morison Forces for Different Sea-States.

The results of these added mass simulations have significant implications for the design and installation of subsea structures. The discrepancies between CFD-derived forces and those predicted by Morison's equation suggest that traditional methods may underestimate or overestimate the hydrodynamic loads during oscillatory flow conditions. This underlines the importance of incorporating CFD-derived coefficients into dynamic simulations, especially for complex installations where added mass and inertia play a substantial role. The challenges posed by negative or varying C_a values also emphasize the need for further research into more sophisticated models that can accurately capture the non-linear fluid-structure interactions in real-world conditions.

In summary, while the use of least squares fitting to Morison's equation provides a useful approximation for added mass effects, it falls short in fully capturing the complex dynamics observed in oscillatory flow. The variability in added mass coefficients and the discrepancies between CFD and fitted forces underscore the need for more advanced modeling techniques. These findings reinforce the value of CFD simulations in providing a more accurate representation of the hydrodynamic forces encountered during installation and operational phases, particularly under challenging high sea-state conditions.

5.4.1. Interpolation Results

The added mass simulations were conducted for three sea states: Sea-state 1, Sea-state 2, and Sea-state 3. In these simulations, three Keulegan-Carpenter (KC) numbers and structural aspect ratios were used to replicate dynamic installation conditions. KC numbers ranged from 0.9 to 0.75, corresponding to frequencies of 1.26 rad/s, 0.90 rad/s, and 0.70 rad/s. In order to apply these simulations to the specific

dimensions of thereal world J-Mode PLET structure, interpolation was carried out using pre-calculated drag forces, drag coefficients (C_d), and added mass coefficients (C_a) derived from these sea states.

This interpolation approach serves as an initial approximation to better understand the dynamic interaction between the subsea structure and oscillatory flows. By leveraging the fitted coefficients from these sea states, a practical solution is developed, providing insight into the range of drag and added mass effects under the given installation conditions. This method forms a bridge between direct simulation results and their application to a wider array of structural configurations, allowing for more tailored analyses specific to the dynamic behavior of the installation.

Table 5.4: Interpolated Coefficients for Added Mass and Drag.

Parameter	**Sea-State**	C_d **Range**	C_a **Range**
Interpolated Value	1, 2, 3	1.08–1.15	0.11–0.56

As indicated in Table 5.4, the interpolated drag coefficient (C_d) and added mass coefficient (C_a) cover a reasonable range across the sea states, reflecting the variability in dynamic conditions. The drag coefficients show minimal variation, staying within a narrow band, whereas the added mass coefficients demonstrate broader fluctuations, highlighting the diverse hydrodynamic interactions at low KC numbers. This interpolation provides a useful approximation, which can serve as a guide for further simulations and experimental validation, particularly when refining models for complex subsea installations.

In summary, the interpolation strategy outlined here demonstrates the value of using simulation-derived coefficients in approximating the hydrodynamic forces in dynamic installation scenarios. The interpolation results serve as an effective foundation for the next stages of detailed simulations, improving the overall understanding of the interactions between oscillatory flows and flow induced motions for submerged subsea structures.

5.5. Dynamic Installation Simulation

The dynamic installation simulations for the J-Mode PLET were performed under various sea-state conditions, incorporating hydrodynamic coefficients derived from both DNV guidelines and CFD interpolations. These simulations aimed to evaluate the structure's response, focusing specifically on bending strains and hydrodynamic mass.

The PLET was modeled with precise dimensions: the longer side (B) was 14.2 m, the shorter side (A) was 13.0 m, and the height was 2.8 m. The perforation ratio of the plate was set at 2.86%, with a water density of 1025 kg/m^3 and a steel density of 7850 kg/m^3. Hydrodynamic coefficients, including a drag coefficient (C_d) of 1.16 from DNV and an interpolated value of 1.08 from CFD simulations, were used to evaluate the structure's behavior. For added mass, DNV guidelines (Table E2, Appendix A, DNV RP H103) provided an added mass coefficient (C_a) of 0.604 for a B/A ratio of 1, with a slamming coefficient of 5. Using these coefficients, the hydrodynamic mass was calculated to be 102.119 tons with the DNV approach and significantly lower using the interpolated coefficients from CFD.

Table 5.5: Interpolated and DNV Coefficients and Hydrodynamic Mass.

Test Case	Source	Drag Coefficient (C_d)	Added Mass Coefficient (C_a)	Hydrodynamic Mass (tons)
1	DNV	1.16	0.604	102.119
2	CFD (Interpolated)	1.08	0.50	84.484
3	CFD (Interpolated)	1.08	0.41	71.474
4	CFD (Interpolated)	1.08	0.30	50.535

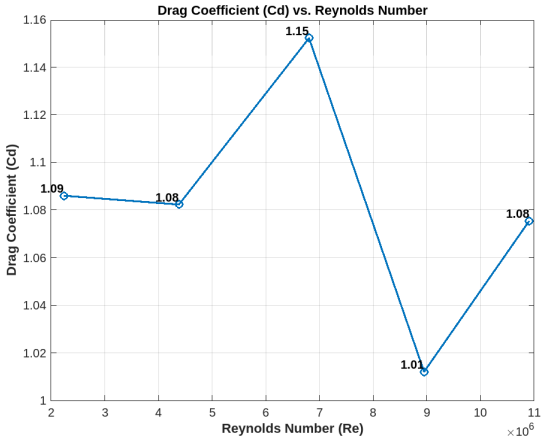

(a) Drag Coefficient (C_d) vs. Reynolds Number

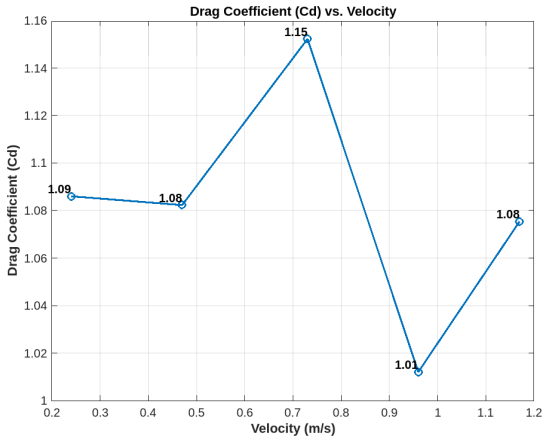

(b) Drag Coefficient (C_d) vs. Velocity

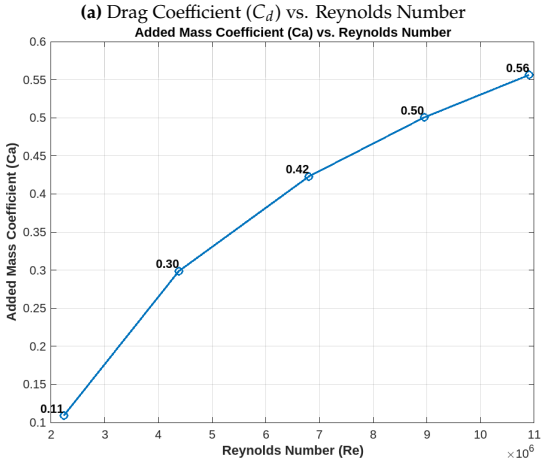

(c) Added Mass Coefficient (C_a) vs. Reynolds Number

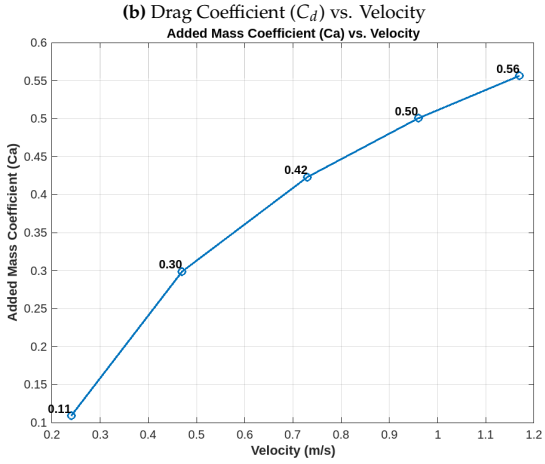

(d) Added Mass Coefficient (C_a) vs. Velocity

Figure 5.22: Interpolated coefficients for added mass and drag as a function of Reynolds number and velocity.

The results of the dynamic installation simulations show a notable reduction in hydrodynamic mass when using CFD-interpolated coefficients compared to DNV values. For instance, in Sea-state 2, the hydrodynamic mass was reduced from 102.119 tons (using DNV) to 50.535 tons (using interpolated $C_a = 0.30$), representing a significant decrease. This reduction in hydrodynamic mass also corresponds to a 10% reduction in bending strains, demonstrating the enhanced accuracy of CFD-derived coefficients in predicting realistic hydrodynamic loads during installation.

The findings validate the use of CFD-interpolated coefficients, which provide more tailored and accurate estimates of hydrodynamic forces compared to traditional DNV guidelines. The advanced CFD models are able to capture more nuanced flow dynamics, such as flow separation and oscillatory effects, which are often simplified or overlooked in empirical methods. As a result, the dynamic simulation framework using CFD values offers a more reliable assessment of subsea structure behavior under varying sea states, leading to improved operational safety and efficiency.

The use of CFD-derived interpolated coefficients in dynamic simulations of the J-Mode PLET demonstrates clear improvements in accuracy, particularly in reducing hydrodynamic mass and bending strains. These findings support the integration of advanced numerical techniques, such as CFD, in the design and installation of subsea structures, where precise prediction of hydrodynamic forces is crucial. The application of this methodology shows that CFD models can effectively complement and refine traditional empirical approaches like DNV, offering a more robust and reliable framework for offshore engineering applications.

6

Conclusions and Recommendations

6.1. Conclusions

The primary objective of this research was to investigate whether integrating Computational Fluid Dynamics (CFD) with traditional guidelines (e.g., DNV) could improve hydrodynamic load predictions for a J-lay Pipeline End Terminal (PLET) installation under higher sea states. The main research question was:

> *Can CFD-based models improve hydrodynamic load predictions for a J-lay Pipeline End Terminal (PLET) installation under higher sea states, improving workability?*

The findings suggest that while CFD-based simulations provide detailed insights into fluid-structure interactions, the overall enhancements over established methodologies remain moderate. Applying CFD-derived coefficients in dynamic installation simulations resulted in a 10% reduction in predicted bending strains in sagbend compared to estimates obtained using DNV values (see section 5.5). This indicates that CFD serves as a supplementary tool, offering refinements rather than a complete replacement of existing industry-standard methodologies. However, the improvements remain case-specific and subject to the limitations of the modeling approach.

The research followed a staged validation process. Initially, 2D simulations were conducted on small-scale thin flat plates, showing agreement with experimental data (section 5.1). This built confidence in the CFD approach's ability to capture fundamental hydrodynamic forces. As the research progressed, full-scale simplified models of mud mats were introduced, first in 2D and later in 3D (subsection 5.3.1). While preliminary 2D simulations provided initial insights, transitioning to 3D simulations became necessary to capture spanwise vortex shedding and realistic flow separations (subsection 4.1.3). These 3D simulations, though computationally demanding, validated the CFD approach under conditions more representative of real subsea environments.

The analysis also considered added mass effects, a transient hydrodynamic factor often simplified in empirical methods. Oscillatory flow simulations on a 3D full-scale mud mat (section 5.4) incorporated standing wave patterns in the fluid domain, enabling added mass coefficient extraction without physically oscillating the structure. Due to computational constraints, only three sets of conditions

were tested (Table 4.9), but interpolation with DNV guidelines allowed estimation across various aspect ratios. The results indicated that CFD-derived added mass coefficients were lower than those from DNV, refining hydrodynamic load estimation.

Incorporating these refined drag and added mass coefficients into dynamic installation simulations (section 5.5) led to the observed 10% reduction in bending strains. This finding underscores the potential of CFD in improving load predictions under certain scenarios.

It is important to emphasize that these outcomes remain preliminary. The models relied on standard turbulence treatments, simplified boundary conditions, and did not fully replicate offshore complexities. The computational intensity constrained the number of tested cases, and while initial validation was promising, more extensive benchmarking remains necessary.

6.1.1. Sub-Research Questions

Validation of 2D CFD Models for Thin Plates: 2D simulations of thin flat plates demonstrated reasonable agreement with experimental data, confirming that the CFD approach could replicate basic hydrodynamic behavior in simplified conditions.

CFD Modeling of Full-Scale Structures: Scaling up to full-scale mud mats and advancing from 2D to 3D simulations highlighted the importance of three-dimensional flow features. Although resource-intensive, 3D simulations provided more realistic load predictions, reinforcing CFD's applicability to complex subsea conditions.

Comparisons with DNV Coefficients and Structural Response: CFD-derived coefficients exhibited trends similar to DNV values but diverged under certain conditions, such as different orientations and aspect ratios. Dynamic simulations incorporating CFD-derived coefficients resulted in a modest reduction in bending strains, indicating CFD's potential refinements over empirical methods.

Impact on Workability: The integration of CFD-derived drag and added mass coefficients improved load predictions, reducing bending strains in dynamic simulations. While these improvements were not transformative, they enhanced the understanding of installation hydrodynamics and informed operational window optimizations.

6.2. Limitations of the Research

Several limitations influenced the interpretation of the results:

- **Environmental Simplifications:** The applied wave theory and boundary conditions did not capture all offshore complexities, such as free-surface effects and seabed interactions.
- **Computational Constraints:** High-fidelity 3D simulations, advanced turbulence models, and broader parametric sweeps were constrained by available computational resources.
- **Modeling Assumptions:** Standard turbulence models and finite mesh resolutions may have overlooked finer flow separations.
- **Partial Validation:** While comparisons with experimental and literature data were positive, they were not exhaustive.

- **Restricted Added Mass Analysis:** Only three flow conditions were tested sinusoidal limiting the generality of interpolations.

6.3. Recommendations for Future Work

To improve the reliability and applicability of CFD-based hydrodynamic modeling:

- **More Realistic Environmental Conditions:** Incorporate free-surface interactions, seabed proximity, and multi-directional wave fields to enhance the representativeness of simulations.
- **Refined Turbulence and Added Mass Modeling:** Utilize Large Eddy Simulation (LES) or hybrid RANS-LES methods for turbulence and expand added mass analysis across a broader range of conditions.
- **Enhanced Mesh and Solver Strategies:** Increase mesh resolution in near-wall regions, explore adaptive meshing techniques, and optimize solver settings to reduce uncertainties.
- **Experimental Validation:** Conduct physical experiments or utilize in-situ field measurements to verify CFD-derived hydrodynamic coefficients.
- **Application to Diverse Structures:** Extend CFD-based methodologies to other subsea structures and operational scenarios to assess broader industry applicability.

6.4. Final Remarks

While this research demonstrated that CFD-based models can provide incremental improvements in hydrodynamic load predictions for subsea installations, the results remain preliminary. Future research should focus on refining computational models, expanding validation efforts, and testing a wider range of sea states and structural configurations. Through continued advancements, CFD has the potential to become a more integral tool in offshore installation planning and design.

References

[1] Mark J Kaiser. "Offshore oil and gas records circa 2020". In: *Ships and Offshore Structures* 17.1 (2022), pp. 205–241.

[2] American Oil Gas Historical Society. "Offshore Drilling History". In: (2023). Accessed: 2024-07-23. URL: https://aoghs.org/offshore-history/offshore-oil-history/.

[3] Philip Pete Stark and Leta K Smith. "Giant oil and gas fields of the 2000s: A new century ushers in deeper water, unconventionals, and more gas". In: (2017).

[4] PetroWiki. "History of Offshore Drilling Units". In: (2023). Accessed: 2024-07-23. URL: https://petrowiki.spe.org/History_of_offshore_drilling_units.

[5] Yong Bai and Qiang Bai. *Subsea Pipeline Design, Analysis, and Installation*. Oxford: Gulf Professional Publishing, 2014. Chap. Installation of Pipelines and Risers, pp. 461–518. ISBN: 9780123868881.

[6] Yong Bai and Qiang Bai. *Subsea engineering handbook*. Gulf Professional Publishing, 2018.

[7] Steinar Thorsen. "Conceptual design and review of Open PLET system". MA thesis. University of Stavanger, Norway, 2012.

[8] GL DNV. "Recommended practice DNVGL-RP-C205 environmental conditions and environmental loads". In: *Høvik: DNV GL AS* (2017).

[9] Allseas Engineering B.V. *Allseas Pipeline Engineering*. 2023.

[10] Det Norske Veritas. *Environmental Conditions and Environmental Loads*. https://rules.dnvgl.com/docs/pdf/DNVGL/RP/2017-07/DNVGL-RP-C205.pdf. DNV GL. 2017.

[11] Odd M. Faltinsen. *Hydrodynamics of High-Speed Marine Vehicles*. Cambridge University Press, 2005.

[12] Det Norske Veritas. *DNV-RP-C205: Environmental Conditions and Environmental Loads*. DNV GL, 2010.

[13] J R Morison, Joseph W Johnson, and Samuel A Schaaf. "The force exerted by surface waves on piles". In: *Journal of Petroleum Technology* 2.05 (1950), pp. 149–154.

[14] Yang Du et al. "Experimental and numerical investigation of hydrodynamic coefficients of subsea manifolds". In: *Ships and Offshore Structures* 16.6 (2021), pp. 595–607.

[15] Chima Clement. "Computational Fluid Dynamics (CFD) Investigation of Hydrodynamic Loading on Subsea Gratings". PhD thesis. UNIVERSITY OF ABERDEEN, 2015.

[16] Tohid Darvishzadeh and Ali Sari. "CFD applications in offshore engineering". In: *Offshore technology conference*. OTC. 2015, OTC–25930.

[17] Chris Kaminsky et al. "A CFD study of wind turbine aerodynamics". In: *Proceedings of the 2012 ASEE North Central Section Conference*. Ohio Northern University. 2012, pp. 1–18.

[18] Yong Bai and Qiang Bai. *Subsea Engineering Handbook*. 2nd. Oxford: Gulf Professional Publishing, 2019. ISBN: 9780128126221.

[19] A. Teixeira, P. Y. M. Low, and S. J. K. Seo. "Report for Subsea Technology". In: *Proceedings of the 20th International Ship and Offshore Structures Congress*. 2018. URL: https://orbi.uliege.be/bitstream/2268/228425/1/Proceedings%20of%20the%2020th%20International%20Ship%20and%20Offshore%20Structures%20Congress%20Volume%202.pdf#page=472.

[20] C. G. J. Nmegbu and L. V. Ohazuruike. "Subsea Technology: a Wholistic View on Existing Technologies and Operations". In: *International Journal of Application or Innovation in Engineering & Management* (2014). URL: https://www.academia.edu/download/34048677/IJAIEM-2014-05-14-037.pdf.

[21] Euroflow Designs. *Escravos Export System Project (EESP): Provision of Diving Support Service, Installation of Mudmats, PLEM, PLMM, SSPR, and Spools*. 2023.

[22] A. N. Umofia. "Risk-based Reliability Assessment of Subsea Control Module for Offshore Oil and Gas Production". PhD thesis. Academia.edu, 2014. URL: https://www.academia.edu/download/87128951/Umofia_Anietie_Thesis_2014.pdf.

[23] Subrata Chakrabarti. *Handbook of Offshore Engineering (2-volume set)*. Elsevier, 2005.

[24] Marwan Darwish and Fadl Moukalled. *The finite volume method in computational fluid dynamics: an advanced introduction with OpenFOAM® and Matlab®*. Springer, 2016.

[25] Chiemela Victor Amaechi, Facheng Wang, and Jianqiao Ye. "Understanding the fluid–structure interaction from wave diffraction forces on CALM buoys: Numerical and analytical solutions". In: *Ships and Offshore Structures* 17.11 (2022), pp. 2545–2573.

[26] Turgut Sarpkaya and James L. O'Keefe. "Oscillating flow about two and three-dimensional bilge keels". In: *Journal of Fluid Mechanics* 1.6 (1996), pp. 1–6.

[27] Maureen McIver and P McIver. "The added mass for two-dimensional floating structures". In: *Wave Motion* 64 (2016), pp. 1–12.

[28] Clarence Jimmy Garrison, V Seetharama Rao, and Richard Hoyd Snider. "Wave interaction with large submerged objects". In: *Offshore Technology Conference*. OTC. 1970, OTC–1278.

[29] Hrvoje Jasak. "CFD analysis in subsea and marine technology". In: *IOP Conference Series: Materials Science and Engineering*. Vol. 276. 1. IOP Publishing. 2017, p. 012009.

[30] X. Zhang et al. "CFD simulation is more accurate compared to analytical and semi-empirical methods for complex shapes". In: *Journal of Marine Science and Engineering* 9.1 (2021), p. 56.

[31] *DNV-RP-C205 Environmental Conditions and Environmental Loads*. Det Norske Veritas (DNV), 2021.

[32] Muk Chen Ong. "CFD applications in offshore engineering". In: *EPJ Web of Conferences*. Vol. 143. EDP Sciences. 2017, p. 01002.

[33] Dominic D Chandar, Bharathi Boppana, and Vasanth Kumar. "A comparative study of different overset grid solvers between openfoam, starccm+ and ansys-fluent". In: *2018 AIAA Aerospace Sciences Meeting*. 2018, p. 1564.

[34] Spyros A Mavrakos. "Hydrodynamic coefficients in heave of two concentric surface-piercing truncated circular cylinders". In: *Applied Ocean Research* 26.3-4 (2004), pp. 84–97.

[35] RS Peterson. "Evaluation of semi-empirical methods for predicting linear static and rotary hydrodynamic coefficients". In: *NCSC TM 291* 80 (1980).

[36] D Humphreys. "Dynamics and hydrodynamics of ocean vehicles". In: *OCEANS 81*. IEEE. 1981, pp. 88–91.

[37] Meyer Nahon. "Determination of undersea vehicle hydrodynamic derivatives using the USAF DATCOM". In: *Proceedings of OCEANS'93*. IEEE. 1993, pp. II283–II288.

[38] Jesse Stuart Geisbert. "Hydrodynamic modeling for autonomous underwater vehicles using computational and semi-empirical methods". PhD thesis. Virginia Tech, 2007.

[39] Khalid Isa, MR Arshad, and Syafizal Ishak. "A hybrid-driven underwater glider model, hydrodynamics estimation, and an analysis of the motion control". In: *Ocean Engineering* 81 (2014), pp. 111–129.

[40] Bas Buchner et al. "A new simulation method for the installation of subsea structures from the splash zone to the ultra deep". In: *DOT conference, November*. 2003, pp. 19–21.

[41] BW Nam, NW Kim, and SY Hong. "Experimental and numerical study on coupled motion responses of a floating crane vessel and a lifted subsea manifold in deep water". In: *International Journal of Naval Architecture and Ocean Engineering* 9.5 (2017), pp. 552–567.

[42] Jinxuan Li et al. "Experimental investigation of the hydrodynamic characteristics of heave plates using forced oscillation". In: *Ocean Engineering* 66 (2013), pp. 82–91.

[43] Xu Liang et al. "Experimental and numerical investigation of the drag coefficients of subsea tree". In: *Ocean Engineering* 238 (2021), p. 109701.

[44] Turgut Sarpkaya. *Morison's equation and the wave forces on offshore structures*. Naval Civil Engineering Laboratory Carmel, CA, USA, 1981.

[45] G.H. Keulegan and L.H. Carpenter. "Forces on cylinders and plates in an oscillating fluid". In: *National Bureau of Standards* (1956).

[46] Garbis Keulegan and Llyod H Carpenter. "Forces on cylinders and plates in an oscillating fluid." In: *US Department of Commerce, national bureau of standards* (1958).

[47] Turgut Sarpkaya. "Force on a circular cylinder in viscous oscillatory flow at low Keulegan—Carpenter numbers". In: *Journal of Fluid Mechanics* 165 (1986), pp. 61–71.

[48] Song An and Odd M Faltinsen. "An experimental and numerical study of heave added mass and damping of horizontally submerged and perforated rectangular plates". In: *Journal of Fluids and Structures* 39 (2013), pp. 87–101.

[49] Tim Bunnik and Bas Buchner. "Experimental investigation of subsea structures during installation and the related wave loads, added mass and damping". In: *ISOPE International Ocean and Polar Engineering Conference*. ISOPE. 2004, ISOPE–I.

[50] Jiasheng Li et al. "Investigation of added mass and damping coefficients of underwater rotating propeller using a frequency-domain panel method". In: *Journal of Sound and Vibration* 432 (2018), pp. 602–620.

[51] Yu-cun Pan, Huai-xin Zhang, and Qi-dou Zhou. "Numerical prediction of submarine hydrodynamic coefficients using CFD simulation". In: *Journal of Hydrodynamics* 24.6 (2012), pp. 840–847.

[52] JFM Gadelho et al. "Heave and sway hydrodynamic coefficients of ship hull sections in deep and shallow water using Navier-Stokes equations". In: *Ocean Engineering* 154 (2018), pp. 262–276.

[53] Likhitha Ramesh Reddy et al. "Validation of CFD determined hydrodynamic coefficients for a semisubmersible floating offshore wind turbine". In: *Journal of Physics: Conference Series*. Vol. 2265. 4. IOP Publishing. 2022, p. 042012.

[54] S. Murthy and M. L. Munjal. *Computational Fluid Dynamics for Engineers and Scientists*. Elsevier, 2018. URL: https://www.elsevier.com/books/computational-fluid-dynamics-for-engineers-and-scientists/9780128046711.

[55] Fredrik Mentzoni, Mia Abrahamsen-Prsic, and Trygve Kristiansen. "Hydrodynamic coefficients of simplified subsea structures". In: *International Conference on Offshore Mechanics and Arctic Engineering*. Vol. 51203. American Society of Mechanical Engineers. 2018, V001T01A034.

[56] Gong Xiang and C Guedes Soares. "A CFD approach for numerical assessment of hydrodynamic coefficients of an inclined prism near the sea bottom". In: *Ocean Engineering* 252 (2022), p. 111140.

[57] Vengatesan Venugopal, KS Varyani, and PC Westlake. "Drag and inertia coefficients for horizontally submerged rectangular cylinders in waves and currents". In: *Proceedings of the Institution of Mechanical Engineers, Part M: Journal of Engineering for the Maritime Environment* 223.1 (2009), pp. 121–136.

[58] Chunqi Wang, Decheng Wan, and Zhaoyun Zong. "Numerical Simulation of Hydrodynamic Forces on a Subsea Pipeline near a Seabed Using OpenFOAM". In: *Ocean Engineering* 154 (2018), pp. 154–164. DOI: 10.1016/j.oceaneng.2018.01.064.

[59] Qingyu Li, Decheng Wan, and Chao Hu. "Numerical Simulation of Wave-Induced Forces on Subsea Pipelines Using OpenFOAM". In: *Ocean Engineering* 127 (2016), pp. 194–204. DOI: 10.1016/j.oceaneng.2016.10.004.

[60] Saurabh Mohapatra and Subrata Kumar Bhattacharyya. "Application of CFD in Offshore Engineering: A Review". In: *Ships and Offshore Structures* 13.3 (2018), pp. 262–277. DOI: 10.1080/17445302.2018.1425908.

[61] H. K. Versteeg and W. Malalasekera. *An Introduction to Computational Fluid Dynamics: The Finite Volume Method*. 2nd. Pearson Education, 2007. ISBN: 9780131274983.

[62] J. H. Ferziger and M. Peric. *Computational Methods for Fluid Dynamics*. Springer, 2002.

[63] H. Schlichting. *Boundary-Layer Theory*. 7th. McGraw-Hill, 1979.

[64] D.C. Wilcox. *Turbulence Modeling for CFD*. DCW Industries, Inc., 1998.

[65] F. R. Menter. "Two-equation eddy-viscosity turbulence models for engineering applications". In: *AIAA Journal* 32.8 (1994), pp. 1598–1605.

[66] *DNVGL-RP-N103 Model Tests and Computer Simulations of Marine Operations*. DNVGL, 2019.

[67] O. M. Faltinsen. *Sea Loads on Ships and Offshore Structures*. Cambridge University Press, 1990.

[68] B. M. Sumer and J. Fredsøe. *Hydrodynamics Around Cylindrical Structures*. World Scientific, 1997.

[69] H Maeda and S Tatsuta. "A STUDY ON THE LINEAR HYDRODYNAMIC FORCES ACTING ON AN UNMANNED UNTETHERED SUBMERSIBLE". In: (1988).

[70] Henrik Mork and Johannes Lunde. "A Cost-Effective and Safe Method for Transportation and Installation of Subsea Structures—The Pencil Buoy Method". In: *SPE Offshore Europe Conference and Exhibition*. SPE. 2007, SPE–108608.

[71] Ehsan Javanmard, Shahriar Mansoorzadeh, and Javad A Mehr. "A new CFD method for determination of translational added mass coefficients of an underwater vehicle". In: *Ocean Engineering* 215 (2020), p. 107857.

[72] Lin Hong et al. "Numerical Study on Hydrodynamic Coefficient Estimation of an Underactuated Underwater Vehicle". In: *Journal of Marine Science and Engineering* 10.8 (2022), p. 1049.

[73] Mia Abrahamsen-Prsic, Frøydis Solaas, and Trygve Kristiansen. "Hydrodynamic Coefficients of Generic Subsea Modules in Forced Oscillation Tests–Importance of Structure Parts". In: *International Conference on Offshore Mechanics and Arctic Engineering*. Vol. 85857. American Society of Mechanical Engineers. 2022, V001T01A019.

[74] Frøydis Solaas et al. "An experimental and numerical study of added mass and damping for side-by-side plates in oscillating flow". In: *Journal of Offshore Mechanics and Arctic Engineering* 143.1 (2021), p. 011901.

[75] Igor Andrade Coutinho et al. "Numerical analysis of the effect of oscillation and current on hydrodynamic coefficients of simple geometries". In: *Ocean Engineering* 283 (2023), p. 115016.

A

Computational Fluid Dynamics

A.1. Governing Equations and Discretization Methods

CFD facilitates the numerical solution of fluid flow equations, enabling the prediction of fluid behavior across various engineering scenarios. By discretizing the governing partial differential equations (PDEs) into algebraic forms, CFD provides approximate solutions, which can be efficiently computed using modern computational resources.

A.1.1. Mass Conservation Equation

The mass conservation equation is a fundamental principle in fluid dynamics, ensuring that the fluid's mass remains constant as it flows. It is mathematically expressed as:

$$\frac{\partial \rho}{\partial t} + \nabla \cdot (\rho \mathbf{u}) = 0 \tag{A.1}$$

This equation guarantees that the mass within a fluid element is conserved as it traverses through the flow field.

A.1.2. Momentum Conservation Equation

The momentum conservation equation, derived from Newton's second law, is given by:

$$\frac{\partial (\rho \mathbf{u})}{\partial t} + \nabla \cdot (\rho \mathbf{u}\mathbf{u}) = -\nabla p + \nabla \cdot \boldsymbol{\tau} + \mathbf{f} \tag{A.2}$$

This equation considers the forces acting on the fluid, encompassing pressure gradients, viscous stresses, and external body forces.

A.1.3. Energy Conservation Equation

The energy conservation equation embodies the energy balance within a fluid element:

$$\frac{\partial(\rho E)}{\partial t} + \nabla \cdot (\rho E \mathbf{u}) = -\nabla \cdot \mathbf{q} + \boldsymbol{\tau} : \nabla \mathbf{u} + q_{\text{ext}} \tag{A.3}$$

In this equation, E denotes the total energy per unit mass, $\mathbf{q}$ represents the heat flux vector, and q_{ext} accounts for external heat sources or sinks.

A.1.4. Discretization Methods

CFD employs discretization methods to solve these equations on a computational grid. Key discretization techniques include:

Finite Difference Method (FDM)

The Finite Difference Method (FDM) approximates derivatives using differences between grid points. For example, the central difference approximation for a derivative is:

$$\frac{du}{dx} \approx \frac{u_{i+1} - u_{i-1}}{2\Delta x} \tag{A.4}$$

Finite Volume Method (FVM)

The Finite Volume Method (FVM) integrates the equations over control volumes, ensuring that conservation laws are satisfied across each discrete volume element. The discretized form of the continuity equation in FVM is:

$$\int_V \frac{\partial \rho}{\partial t} dV + \int_S \rho \mathbf{u} \cdot \mathbf{n} dS = 0 \tag{A.5}$$

Finite Element Method (FEM)

The Finite Element Method (FEM) uses variational principles to approximate solutions over a mesh of elements. For example, the weak form of Poisson's equation is:

$$\int_\Omega \nabla v \cdot \nabla u \, d\Omega = \int_\Omega v f \, d\Omega \tag{A.6}$$

In this equation, Ω represents the domain, v is a test function, and f is a source term.

A.1.5. Wall Modeling in Turbulent Flows

Wall modeling is essential in CFD simulations, particularly for high Reynolds number flows where accurate near-wall resolution is critical. The flow near the wall is divided into different regions, each requiring specific modeling techniques:

- **Viscous Sublayer:** The region closest to the wall where viscous effects dominate, typically within $y^+ < 5$, where y^+ is the dimensionless wall distance.
- **Log-Law Region:** The region within $30 < y^+ < 200$, where the velocity profile follows a logarithmic distribution, marking the transition to fully developed turbulence.
- **Outer Region:** The area beyond the logarithmic region where the flow becomes fully turbulent and the wall's influence diminishes.

Viscous Sublayer Resolving Approach

The viscous sublayer resolving approach places the first grid point very close to the wall, typically at $y^+ \approx 1$, ensuring full resolution of the viscous sublayer. This method requires a fine mesh near the wall, which increases computational costs but provides high accuracy in near-wall flow predictions.

The dimensionless velocity u^+ and the dimensionless wall distance y^+ are defined as:

$$u^+ = \frac{U}{U_\tau}, \quad y^+ = \frac{yU_\tau}{\nu} \tag{A.7}$$

Where U is the velocity at a distance y from the wall, and U_τ is the friction velocity, given by $U_\tau = \sqrt{\tau_w/\rho}$, where τ_w is the wall shear stress and ρ is the fluid density.

This approach resolves the velocity profile near the wall directly, offering a detailed understanding of the boundary layer characteristics, crucial for simulations where accurate wall shear stress predictions are necessary.

Logarithmic-Based Wall Function Approach

The logarithmic-based wall function approach positions the first grid point in the logarithmic layer, around $y^+ \approx 30$. This method uses semi-empirical functions to model the near-wall region, reducing the need for a fine mesh near the wall, thereby lowering computational costs.

The logarithmic law of the wall is expressed as:

$$u^+ = \frac{1}{\kappa} \ln y^+ + B \tag{A.8}$$

Where κ is the von Kármán constant, approximately 0.41, and B is an empirical constant, typically around 5.0 for smooth walls.

This approach is suited for high Reynolds number flows, where the flow near the wall is fully turbulent, and the viscous sublayer occupies a smaller portion of the boundary layer. By using wall functions, computational effort is reduced while still capturing essential features of the turbulent boundary layer.

A.1.6. Hybrid Models: Detached Eddy Simulation (DES)

Detached Eddy Simulation (DES) is a hybrid modeling technique that combines the advantages of Reynolds-Averaged Navier-Stokes (RANS) models and Large Eddy Simulation (LES). DES uses RANS modeling near the wall, where the flow is dominated by small-scale turbulence, and LES in regions where large-scale turbulence structures are significant.

The governing equations for DES are based on the filtered Navier-Stokes equations, similar to LES, with additional terms to manage the transition between RANS and LES:

$$\frac{\partial \overline{u}_i}{\partial t} + \overline{u}_j \frac{\partial \overline{u}_i}{\partial x_j} = -\frac{1}{\rho} \frac{\partial \overline{p}}{\partial x_i} + \nu \frac{\partial^2 \overline{u}_i}{\partial x_j^2} + \frac{\partial \tau_{ij}}{\partial x_j} \tag{A.9}$$

Where $\overline{u}_i$ is the filtered velocity component, $\overline{p}$ is the filtered pressure, ν is the kinematic viscosity, and τ_{ij} represents the subgrid-scale stresses, modeled in the LES region.

DES effectively addresses the challenges of simulating large-scale turbulent structures without the high computational costs of full LES. It is particularly beneficial in flows with significant separation or large-scale vortex shedding, such as in the wake of bluff bodies or in aerodynamic applications.

A.2. Turbulence Modeling and Simulation Approaches

Turbulence modeling is a critical aspect of CFD simulations, particularly in marine and offshore engineering applications. The accurate representation of turbulent flows, which are prevalent in most fluid dynamics scenarios, significantly influences the predictions of complex fluid behaviors, such as those encountered around subsea structures. Various models are employed depending on the desired accuracy and the computational resources available.

A.2.1. Direct Numerical Simulation (DNS)

DNS resolves all scales of turbulence by directly solving the Navier-Stokes equations without any turbulence modeling, offering the highest level of detail. However, this approach is computationally expensive and typically reserved for fundamental research or very small-scale problems. The governing equations for DNS are:

$$\frac{\partial \rho}{\partial t} + \nabla \cdot (\rho \mathbf{u}) = 0 \tag{A.10}$$

$$\frac{\partial (\rho \mathbf{u})}{\partial t} + \nabla \cdot (\rho \mathbf{u}\mathbf{u}) = -\nabla p + \nabla \cdot \boldsymbol{\tau} + \mathbf{f} \tag{A.11}$$

A.2.2. Large Eddy Simulation (LES)

LES resolves the larger scales of turbulence and models the smaller scales using subgrid-scale models. This approach provides more detail than RANS while being less computationally expensive than DNS. LES is particularly effective in capturing transient and unsteady flows, such as vortex shedding, and is widely used in engineering applications where such phenomena are critical. The governing equations for LES are:

$$\frac{\partial \overline{\rho}}{\partial t} + \nabla \cdot (\overline{\rho} \mathbf{u}) = 0 \tag{A.12}$$

$$\frac{\partial (\overline{\rho} \mathbf{u})}{\partial t} + \nabla \cdot (\overline{\rho} \mathbf{u}\mathbf{u}) = -\nabla \overline{p} + \nabla \cdot \overline{\boldsymbol{\tau}} + \overline{\mathbf{f}} \tag{A.13}$$

A.2.3. Reynolds-Averaged Navier-Stokes (RANS)

RANS models involve time-averaging the Navier-Stokes equations, where all turbulent scales are modeled through turbulence models such as the k-ϵ and k-ω models. RANS is widely used in industrial applications due to its relatively low computational cost and ability to provide reasonable accuracy for a wide range of turbulent flows. The time-averaged Navier-Stokes equations are:

$$\frac{\partial (\rho \overline{u}_i)}{\partial t} + \frac{\partial (\rho \overline{u}_i \overline{u}_j)}{\partial x_j} = -\frac{\partial \overline{p}}{\partial x_i} + \frac{\partial}{\partial x_j} \left(\mu \frac{\partial \overline{u}_i}{\partial x_j} - \rho \overline{u_i' u_j'} \right) \tag{A.14}$$

In these equations, $\overline{u_i' u_j'}$ represents the Reynolds stress, which must be modeled to close the equations.

A.2.4. k-ϵ and k-ω Models

The k-ϵ and k-ω models are widely used for providing closure to the RANS equations by introducing additional transport equations for turbulence kinetic energy (k) and its dissipation rate (ϵ) or specific dissipation rate (ω).

k-ϵ Model:

$$\frac{\partial(\rho k)}{\partial t} + \nabla \cdot (\rho k \mathbf{u}) = \nabla \cdot \left(\left(\mu + \frac{\mu_t}{\sigma_k} \right) \nabla k \right) + P_k - \rho \epsilon \tag{A.15}$$

k-ω Model:

$$\frac{\partial(\rho \omega)}{\partial t} + \nabla \cdot (\rho \omega \mathbf{u}) = \nabla \cdot \left(\left(\mu + \frac{\mu_t}{\sigma_\omega} \right) \nabla \omega \right) + P_\omega - \rho \beta^* \omega^2 \tag{A.16}$$

Table A.1: Comparison of Turbulence Models

Turbulence Model	Advantages	Limitations	Applications
k-ϵ Model	Simple, computationally efficient	Sensitive to free-stream turbulence	Industrial flows
k-ω SST Model	Accurate near walls, robust	Limited performance in separating flows	General purpose
LES	Captures large turbulent structures	High computational cost	Unsteady flows
DES	Combines RANS and LES benefits	Sensitivity to grid resolution	Complex flows

A.2.5. Governing Equations for Turbulence Models

Understanding the mathematical foundation of turbulence models is essential for selecting the appropriate model for a given application. Below are the governing equations for some of the most commonly used turbulence models in CFD.

Table A.2: Governing Equations for Turbulence Models

Turbulence Model	Governing Equations
k-ϵ Model	$\frac{\partial(\rho k)}{\partial t} + \nabla \cdot (\rho k \mathbf{u}) = \nabla \cdot \left[\left(\nu + \frac{\nu_t}{\sigma_k} \right) \nabla k \right] + G_k - \rho \varepsilon$ $\frac{\partial(\rho \varepsilon)}{\partial t} + \nabla \cdot (\rho \varepsilon \mathbf{u}) = \nabla \cdot \left[\left(\nu + \frac{\nu_t}{\sigma_\varepsilon} \right) \nabla \varepsilon \right] + C_{\varepsilon 1} \frac{\varepsilon}{k} (G_k - C_{\varepsilon 2} \rho \varepsilon)$
k-ω SST Model	$\frac{\partial(\rho k)}{\partial t} + \nabla \cdot (\rho k \mathbf{u}) = \nabla \cdot \left[\left(\nu + \frac{\nu_t}{\sigma_k} \right) \nabla k \right] + G_k - \beta^* \rho \omega$ $\frac{\partial(\rho \omega)}{\partial t} + \nabla \cdot (\rho \omega \mathbf{u}) = \nabla \cdot \left[\left(\nu + \frac{\nu_t}{\sigma_\omega} \right) \nabla \omega \right] + \beta \rho \omega^2 + (1 - \beta) \rho \varepsilon$
LES	$\frac{\partial \bar{\rho}}{\partial t} + \nabla \cdot (\bar{\rho} \mathbf{u}) = 0$ (Continuity) $\frac{\partial(\bar{\rho} \mathbf{u})}{\partial t} + \nabla \cdot (\bar{\rho} \mathbf{u} \mathbf{u}) = -\nabla \bar{P} + \nabla \cdot \bar{\bar{\tau}} + \bar{\rho} \mathbf{g}$ (Momentum)
DES	RANS-near-wall region, LES-away from the wall

Explanation of the Equations:

- **k-ϵ Model:** The k-ϵ model solves two separate transport equations: one for the turbulence kinetic energy (k) and another for the rate of dissipation of turbulence kinetic energy (ϵ). The advantage of this model lies in its simplicity and robustness for a wide range of flows. However, its accuracy diminishes in flows with high curvature, separation, or strong pressure gradients.
- **k-ω SST Model:** The k-ω SST model combines the advantages of the k-ϵ model in the free stream and the k-ω model near walls. This model is known for its accuracy in predicting boundary layer flows and separation points, making it a preferred choice for complex flow situations.
- **LES:** The Large Eddy Simulation (LES) approach resolves the larger scales of turbulence directly and models the smaller scales. LES is particularly effective in capturing the dynamic behavior of turbulent flows, though at a higher computational cost.
- **DES:** Detached Eddy Simulation (DES) is a hybrid approach that combines RANS and LES. DES applies RANS modeling in regions where the grid resolution is coarse and LES in areas with fine grid resolution. This approach provides a good balance between computational efficiency and accuracy.

B

Summary of research Articles

B.0.1. General List of Research Articles

The general list of research articles (Table B.1) covers a broad range of studies on hydrodynamic load models, offering insights into various methodologies and flow conditions. These articles span across analytical, experimental, and numerical approaches, illustrating the evolution of techniques over the years. The key takeaways from these studies include the importance of method selection based on the specific flow conditions and the type of structure under consideration.

Table B.1: General List of Research Articles on Hydrodynamic Load Models

Year	Publisher	Methodology	Type of Flow	Turb Model	Key Findings
1980	Peterson [35]	Semi-Analytical	Steady	N/A	Evaluated hydrodynamic coefficients using empirical techniques
1981	Humphreys [36]	Semi-Analytical	Steady	N/A	Studied flow around underwater vehicles
1988	Maeda [69]	Semi-Analytical	Steady	N/A	Utilized empirical techniques for underwater vehicles
1993	Nahon [37]	Semi-Analytical	Steady	N/A	Determined hydrodynamic coefficients for underwater vehicles
2004	Mavrakos et al. [34]	Analytical	Unsteady	N/A	Investigated linearized hydrodynamic radiation for vertical cylinders
2007	Giesbert [38]	Semi-Analytical	Steady	N/A	Used equations of motion for autonomous underwater vehicles
2007	Mork [70]	Empirical	Steady	N/A	Developed cost-effective method for transportation and installation of subsea structures
2014	Isa [39]	Semi-Analytical	Steady	N/A	Used hybrid model combining empirical and numerical methods for estimating hydrodynamic coefficients
2016	McIver et al. [27]	Analytical	Unsteady	N/A	Examined added mass properties of surface-piercing structures
2018	Li et al. [50]	Numerical	Unsteady	k-ϵ	Developed numerical method to estimate added mass and damping coefficients
2020	Javanmard et al. [71]	Experimental	Unsteady	N/A	Investigated hydrodynamic performance in complex environments
2022	Hong et al. [72]	Numerical	Steady	k-ω SST	Numerical analysis of hydrodynamic coefficients for underwater vehicles

Specific Research Articles on Submerged and Subsea Structures

The specific list of research articles (Table B.2) delves into the studies that directly address submerged and subsea structures, focusing on the estimation of hydrodynamic coefficients such as drag, added mass, and damping. These studies employ a mix of experimental, numerical, and hybrid methods, underscoring the importance of accurate coefficient estimation for design and operational performance in marine environments.

Table B.2: Research Articles on Hydrodynamic Coefficients for Submerged/Subsea Structures

Year	Publisher	Methodology	Type of Flow	Turbulence Model	Key Findings
2003	Buchner et al. [40]	CFD, Experimental	Unsteady	N/A	Developed a methodology for predicting response of subsea structures in the splash zone and combined numerical simulations with model tests to derive drag coefficients and explored the effects of KC number on hydrodynamic coefficients.
2012	Pan [51]	RANS Simulations, PMM Experiments	Unsteady	k-ω SST	Predicted hydrodynamic coefficients of an underwater submarine and utilized dynamic mesh techniques to simulate maneuvering, compared simulation results with experimental data, and analyzed the impact of oscillation frequencies on hydrodynamic behavior.
2013	Bunnik et al. [49]	Experimental	Unsteady	N/A	Estimated wave loads, added mass, and damping in the splash zone. Conducted decay and captive tests to determine hydrodynamic coefficients and analyzed the structural response in various immersion states.
2013	An et al. [48]	Experimental, Numerical	Unsteady	k-ϵ	Studied the heave motion of perforated plates in different submergence conditions. Combined potential flow theory with empirical techniques, and employed BEM for inner domain analysis for validation.
2017	Nam et al. [41]	Experimental	Unsteady	N/A	Explored coupled motion responses during deep-water installation. Analyzed dynamic tension in hoisting wires under varying wave conditions and assessed the impact of passive heave compensators on motion and tension responses.
2018	Li et al. [42]	Experimental	Unsteady	N/A	Investigated heave plates of Spar platforms. Conducted forced oscillation tests to study the effects of KC number, oscillation frequency, and perforation on hydrodynamic coefficients.
2018	Gadelho et al. [52]	CFD	Unsteady	k-ω SST	Determined hydrodynamic coefficients of ship hull sections. Employed time-domain Navier-Stokes CFD model, highlighted discrepancies in vortex shedding regions, and compared results with potential flow theory.
2021	Du et al. [14]	CFD	Unsteady	k-ω SST	Studied hydrodynamic coefficients of subsea manifolds. Used CFD simulations validated by experimental tests, found linear relationship between added mass coefficients and KC number, and identified minimal influence of oscillation frequency on drag coefficients.

These summarized studies provide a critical foundation for understanding the complexities of hydrodynamic loading on submerged and subsea structures. The findings emphasize the varied approaches—ranging from empirical and analytical models to advanced CFD simulations—and their respective strengths and limitations. In the context of this thesis, the integration of these methodologies aids in bridging the gaps between traditional empirical methods, as outlined in DNV codes, and advanced numerical simulations, thereby enhancing the accuracy and reliability of hydrodynamic force predictions during subsea installations.

B.1. Hydrodynamic Coefficients

B.1.1. Empirical and Analytical Methods

Empirical methods provide quick and straightforward estimates of hydrodynamic coefficients based on established correlations from experimental data. Although these methods are widely used for their simplicity, they often lack accuracy when applied to complex geometries or flow conditions not covered by the original datasets. Analytical methods, on the other hand, offer fundamental insights into fluid-structure interactions by solving simplified theoretical models. However, their application is often limited by the assumptions made, such as potential flow or idealized boundary conditions, which may not fully capture the complexities of real-world subsea environments.

Table B.3: Comparison of Empirical and Analytical Methods for Estimating Hydrodynamic Coefficients.

Aspect	Empirical Methods	Analytical Methods
Overview	Relies on experimental data to derive correlations. Quick and easy to use but less accurate for complex conditions.	Involves theoretical modeling of fluid flow. Provides insights but often oversimplifies real-world scenarios.
Advantages	Fast and practical for initial estimates.	Useful for understanding basic principles and idealized conditions.
Disadvantages	Limited applicability to specific conditions; lower accuracy.	Often neglects complex fluid interactions and boundary effects.
Typical Applications	Preliminary design, validation of numerical models.	Idealized problems, theoretical studies.

B.1.2. Experimental Methods

Experimental methods are invaluable for obtaining direct measurements of hydrodynamic forces under controlled conditions. These methods provide essential validation for theoretical models and numerical simulations, offering empirical data for various configurations and flow conditions. Common experimental techniques include wind tunnel testing, water flumes, and tow tank testing, each providing unique insights into the hydrodynamic behavior of structures.

Table B.4: Experimental Methods for Estimating Hydrodynamic Coefficients

Aspect	Wind Tunnel Testing	Water Flumes and Tow Tanks
Overview	Simulates airflow around scaled models. Useful for aerodynamic and hydrodynamic studies with appropriate scaling.	Direct measurement of forces in controlled water flow conditions. Commonly used for marine and offshore structures.
Advantages	Provides high accuracy and detailed force measurements.	Allows study of real flow conditions and force interactions on models.
Disadvantages	Requires careful scaling and consideration of Reynolds number effects.	High cost, time-consuming, and scaling issues when replicating full-scale conditions.
Applications	Preliminary design and validation of theoretical/numerical models.	Detailed study of hydrodynamic forces on submerged/subsea structures.

B.1.3. Numerical Methods

Numerical methods, particularly Computational Fluid Dynamics (CFD), have become increasingly popular for predicting hydrodynamic coefficients due to their ability to model complex fluid-structure interactions with high accuracy. CFD allows for detailed analysis of flow fields and force distributions around submerged structures, offering insights that are difficult to obtain experimentally.

Table B.5: Numerical Methods for Estimating Hydrodynamic Coefficients

Aspect	CFD (Computational Fluid Dynamics)	BEM (Boundary Element Method) / FEM (Finite Element Method)
Overview	Solves Navier-Stokes equations for detailed simulation of fluid flow around structures.	Uses boundary and volume discretization to solve potential and flow equations.
Advantages	High accuracy, captures detailed flow features, adaptable to various conditions.	Efficient for specific problems like potential flow; lower computational cost for simple boundaries.
Disadvantages	Computationally intensive, requires expertise in mesh generation and solver settings.	Less effective for highly nonlinear problems or complex geometries.
Applications	Detailed hydrodynamic analysis, validation against experimental results.	Idealized flow problems, initial design assessments.

This section has reviewed the primary methods used for estimating hydrodynamic coefficients of submerged and subsea structures, highlighting the strengths and limitations of empirical, analytical, experimental, and numerical approaches. The choice of method often depends on the specific requirements of the project, including the complexity of the flow conditions, the desired accuracy, and available resources. Numerical methods, particularly CFD, stand out for their ability to provide detailed insights and high accuracy, although they come with increased computational demands.

B.1.4. Studies on Hydrodynamic Coefficients

Table B.6: Summary of studies on hydrodynamic coefficients and forces

Study Title	Objective	Methodology	Key Findings
Hydrodynamic coefficients for simplified subsea structures [55]	Investigate hydrodynamic coefficients of simplified subsea structures.	Experimental testing of 2D models representing components like porous plates and cylindrical pipes.	Vertical hydrodynamic forces were larger than horizontal forces. Waves modified the frequency and position of vortex shedding around the cylinder.
Drag and inertia coefficients for horizontally submerged rectangular cylinders in waves and currents [57]	Study interaction between a submerged solid structure and current with surface waves.	Small-scale flume experiments on submerged rectangular cylinder subjected to current, regular waves, and combined wave-current conditions.	Vertical hydrodynamic forces were larger than horizontal forces. Waves modified the frequency and position of vortex shedding, leading to distinct modes in the frequency domain of vertical force.
Hydrodynamic coefficients of generic subsea modules in forced oscillation tests [73]	Investigate hydrodynamic coefficients of simplified subsea structures through forced oscillation tests.	Experimental tests emphasizing amplitude dependency of coefficients.	Damping is the dominant hydrodynamic force; internal content increases the importance of added mass. Insights aid in improving accuracy of force predictions for subsea installations.
A CFD approach for numerical assessment of hydrodynamic coefficients of an inclined prism near the sea bottom [56]	Compute hydrodynamic coefficients for high-speed vessels in shallow waters.	Steady and unsteady RANS simulations using a sliding mesh model.	Shallow water depths and varying bathymetry impact added mass, viscous damping, and current drag coefficients. Highlights effectiveness of CFD in marine structure design.
Validation of CFD determined hydrodynamic coefficients for a semisubmersible floating offshore wind turbine [53]	Validate CFD results against experimental data for a semisubmersible FOWT.	STAR-CCM+ simulations compared with wave tank experiments.	CFD accurately predicts hydrodynamic coefficients; viscous effects are crucial for accurate drag force estimation. Further validation with full-scale models is suggested.
An experimental and numerical study of added mass and damping for side-by-side plates in oscillating flow [74]	Investigate hydrodynamic behavior of side-by-side plates under oscillating flow conditions.	Experimental and numerical methods using forced harmonic oscillations.	Larger oscillation amplitudes lead to significant hydrodynamic interactions between plates. Accurate modeling of added mass and damping is essential for predicting hydrodynamic forces.
Experimental and numerical investigation of the drag coefficients of subsea tree [43]	Study drag forces acting on subsea trees through experimental and numerical approaches.	Drag tests in a towing tank and CFD simulations.	Drag coefficients are influenced by the complex geometry of subsea trees and flow conditions. Importance of combining experimental and numerical approaches for accurate modeling is emphasized.
Numerical analysis of the effect of oscillation and current on hydrodynamic coefficients of simple geometries [75]	Investigate hydrodynamic behavior of simple geometries subjected to oscillatory motion and steady currents.	CFD simulations using RANS equations to model flow around spheres and cylinders.	Hydrodynamic coefficients are influenced by both oscillation amplitude and current velocity. Combined flow conditions are critical for accurate analysis of marine structures.